HHS Public Access

Author manuscript

Pain. Author manuscript; available in PMC 2024 July 01.

Published in final edited form as:

Pain. 2023 July 01; 164(7): 1473–1488. doi:10.1097/j.pain.0000000000002850.

Targeting the VEGF-A/Neuropilin 1 axis for relief of neuropathic pain

Harrison J. Stratton[4], **Lisa Boinon**[4], **Kimberly Gomez**[1,2], **Laurent Martin**[3], **Paz Duran**[1,2], **Dongzhi Ran**[4], **Yuan Zhou**[4], **Shizhen Luo**[4], **Samantha Perez-Miller**[1,2], **Marcel Patek**[5], **Mohab M. Ibrahim**[3], **Amol Patwardhan**[3], **Aubin Moutal**[6], **Rajesh Khanna**[1,2,*]

[1]Department of Molecular Pathobiology, College of Dentistry, New York University, New York, New York, United States of America

[2]NYU Pain Research Center, 433 First Avenue, New York, NY 10010, United States of America

[3]Department of Anesthesiology, College of Medicine, The University of Arizona; Tucson, Arizona, 85724 United States of America.

[4]Department of Pharmacology, College of Medicine, The University of Arizona; Tucson, Arizona, 85724 United States of America.

[5]BrightRock Path, LLC, Tucson, Arizona 85704, United States.

[6]Saint Louis University - School of Medicine, Department of Pharmacology and Physiology, 1402 S. Grand Blvd., Schwitalla Hall, Room 432, Saint Louis, MO 63104

1.0 – Introduction

Chronic pain is debilitating with significant societal burden and few treatments [36; 65]. An over-reliance on opioids can result in unwanted side effects, including respiratory depression, constipation, and abuse liability [6; 12]. The pathophysiology of chronic pain is highly heterogenous. One common factor shared among chronic pain subtypes is ectopic firing of nociceptive sensory neurons [14; 33] caused by upregulation of voltage-gated ion channels (e.g. NaV1.7 and CaV2.2 [13; 39]). External injury triggers release of inflammatory mediators, which, by coupling to downstream signaling effectors, triggers upregulation of ion channels. One such mediator, originally discovered in the framework of angiogenesis, is vascular endothelial growth factor-A (VEGF-A) [17]. Release of VEGF-A triggers vascularization and angiogenesis, and relevant to tumor growth and cancer [63; 67]. This has led to the development of VEGF-targeting therapies for cancers and to prevent tissue hypertrophy; the latter may contribute to chronic pain and may be related to local

*To whom correspondence should be addressed: Dr. Rajesh Khanna, Department of Molecular Pathobiology, College of Dentistry, New York University, 433 1st Avenue Room 822 New York City, NY 10010 rk4272@nyu.edu.

‡Contributed equally

Author Contributions –

R.K. developed the concept, designed the experiments, and supervised all aspects of this project. H.S. and L.B. collected electrophysiology data. H.S. wrote the manuscript. R.K. and A.M. designed and supervised experiments and advised in data analysis. P.D, K.G., D.R., Y.Z., L.M., collected and analyzed the data. S.P.-M performed docking studies of the compound. M.P. assisted with compound selection and medicinal chemistry. H.S., L.B., K.G., D.R., Y.Z., performed electrophysiological recordings. S.L. and L.M performed behavioral experiments. R.K. supervised all aspects of this project. All authors had the opportunity to discuss the results and comment on the manuscript.

release of VEGF-A. Once released, VEGF-A binds to one of two receptor tyrosine kinases — VEGF-R1 or VEGF-R2 [54]. These receptors can form complexes with other cell surface receptors, such as Neuropilin 1 (NRP1).

While divergent in function, vascular and neuronal systems are often anatomically parallel with these tissues sharing many common cellular/molecular mechanisms [9]. One such point of similarity between the vascular and nervous systems is VEGF-A. Alongside its role in regulating vascular processes, VEGF-A directly modulates neuronal function through VEGF-R2 activation. Notably, VEGF-A modulates neurotransmission and synaptic plasticity, through facilitation of long-term potentiation [16; 44]. Since VEGF-A is important for neurotransmission, it is reasonable to conclude that this factor could be involved in pain signaling. Prior reports have linked VEGF-A and chronic pain states, such as cancer-induced bone pain and inflammatory conditions like rheumatoid arthritis and osteoarthritis [24; 30; 38; 64]. While investigating severe acute respiratory syndrome coronavirus 2 (SARS-CoV-2), two studies reported that the virus's Spike protein — responsible for viral entry through interactions with the Angiotensin-converting enzyme 2 receptor — could also bind NRP1 [8] and interrupt VEGF-A binding to NRP1 [15]. Based on these findings, we showed VEGF-A to be a pro-nociceptive signaling factor through its interaction with NRP1 [51]. Inhibition of VEGF-A/NRP-1 binding using either SARS-CoV2 Spike protein or a commercially available NRP1 inhibitor EG00229 [35] reversed experimental neuropathic pain [51].

Capitalizing on our discovery of this novel VEGF-A/NRP1 pain axis, we screened for compounds that could prevent binding of VEGF-A to NRP1 and could be developed into treatments for chronic pain [55]. We reasoned that blocking the binding between VEGF-A and NRP1 would reduce the pro-nociceptive action mediated by VEGF-A activation. We identified six compounds that inhibited the VEGF-A/NRP1 interaction more potently than EG00229 [55]. Here, we examined the *in vitro* and *in vivo* mechanism of action of the lead compound 4'-methyl-2'-morpholino-2-(phenylamino)-[4,5'-bipyrimidin]-6(1H)-one (NRP1–4), and its effect on mitigating pain. We show that NRP1–4 blocked VEGF-A induced enhancement of sodium and N-type calcium currents and reverses experimental neuropathic pain in two different preclinical pain models.

2.0 – Materials and Methods

2.1 – Docking of NRP1–4 to VEGF-A binding domain of NRP1

The highest resolution structure of the NRP-1 b1 domain was selected for docking (PDB code 6fmc) [56]. This structure was prepared using the Protein Preparation Wizard88 to remove all water molecules and alternate conformations, add and refine hydrogen atoms, and conduct restrained minimization (OPLS3e force field, convergence to 0.30 Å) [61]. There were no residues with alternate conformations within the binding pocket. A 20 Å × 20 Å × 20 Å grid box was centered on the co-crystallized inhibitor EG01377 to target the VEGF-A_{165} site. An optional, symmetric constraint was generated that required hit compounds to form a hydrogen bond to the sidechain of Asp 320. Docking was run against the VEGF-A_{165} binding site of NRP-1 using Glide XP (Schrödinger, LLC, New York, NY, 2020) [26].

2.2 – Animals

Pathogen-free, adult male and female Sprague-Dawley rats (100–250 g, Envigo, Placentia, CA) were kept in light (12-h light: 12-h dark cycle; lights on at 07:00 h) and temperature (23 ± 3°C) controlled rooms, with standard rodent chow and water ad libitum. Pathogen-free, male Sprague Dawley rat pups (postnatal 10–15 days; Envigo, Placentia, CA) were used for electrophysiological recordings in spinal cord slices. All animal use was conducted in accordance with the National Institutes of Health guidelines, and the study was conducted in strict accordance with recommendations in the Guide for the Care and Use of Laboratory Animals of the University of Arizona (Protocol #: 16–141). All efforts were made to minimize animal suffering. All behavioral experiments were performed by experimenters who were blinded to the genotype, and sex, and treatment groups.

2.3 Reagents

All chemicals, unless noted, were purchased from Sigma (St Louis, MO). All compounds screened in our lab are initially dissolved in DMSO for in vitro characterization to allow for uniform conditions across molecular species. NRP1–4 was dissolved in pure DMSO at a concentration of 12.5 uM and VEGF-A (Fisher Scientific, #89–967-005) resuspended in PBS to a stock concentration of 1 μM to allow further dilution to either 1 or 4 nM. For in vivo applications NRP1–4 was first prepared as a stock solution in DMSO and then diluted in phosphate buffered saline for either intrathecal injection or intravenous injection. The final concentration of DMSO in these solutions was kept at 0.1% to be consistent between in vitro and in vivo studies. Previous studies have shown that DMSO is a suitable solvent for use in delivery of experimental compounds to the CNS [5].

2.4 – Isolation and culture of rodent DRG neurons

Female Sprague-Dawley rats (100g) were obtained from Envigo and euthanized according to institutionally approved procedures. Skin, muscle and vertebrae were cut to expose lumbar and thoracic dorsal root ganglia (DRG) as previously described [49]. Nerve roots were trimmed and DRGs were carefully removed and placed in DMEM (Cat# 11965; Life technologies, Carlsbad, CA)) and digested for 1 hour at 37°C under gentle agitation with 3.125mg/mL protease and 5mg/mL collagenase (#LS021104 and #LS004194, Worthington Biochemical Corp.). Dissociated cells were pelleted by centrifugation for 3 minutes at 800g at 25°C, resuspended in DMEM containing 10% fetal bovine serum (Cat#S11150; R&D Systems, Minneapolis, MN), 30 ng/mL nerve growth factor, penicillin and streptomycin (100 U/mL and 100μg/mL) and plated on poly- D-lysine-coated 12mm coverslips. Neurons were then used for electrophysiological recordings to investigate action potential firing and measurement of voltage-gated ion channel currents.

2.5 – Electrophysiological recordings from rodent DRG neurons

All recordings were obtained from acutely dissociated DRG neurons from Sprague Dawley rats and pigs, using procedures adapted from our prior work [22; 23; 34]. Recordings were performed from neurons with a capacitance value below 30 pF, which has been historically associated with the population of small diameter c-fiber nociceptive neurons within the DRG [2]. DRG neurons were incubated for 30 min with either 0.1% DMSO, VEGF-A (1 nM)

or NRP1–4 (12.5 μM).For sodium current recordings the internal pipette solution consisted of (in mM): 140 CsF, 10 NaCl, 1.1Cs-EGTA, and 15 HEPES (pH 7.3, mOsm/L = 290–310) and external solution contained (in mM): 140 NaCl, 30 tetraethylammonium chloride, 10 D-glucose, 3 KCl, 1 CaCl2, 0.5 CdCl2, 1 MgCl2, and 10 HEPES (pH 7.3, mOsm/L = 310–315). DRG neurons were interrogated with current-voltage (I-V) and activation/inactivation voltage protocols as described previously [25]. The voltage protocols were as follows: (a) I-V protocol: from a holding potential of −60 mV, cells were depolarized with 150-millisecond voltage steps over a range of −70 to +60 mV in +5 - mV increments. This permitted acquisition of current density values such that the activation of sodium channels, occurring between ~0 to 10 mV, could be analyzed as a function of voltage, from which peak current density was inferred (normalized to cell capacitance (in picofarads, pF)); (b) inactivation protocol: from a holding potential of −60 mV, cells were subjected to hyperpolarizing/repolarizing pulses for 1 second over a range of −120 to 0 mV in +10 mV steps. This incremental increase in membrane potential conditioned various proportions of sodium channels into a state of fast-inactivation – in this case the 0-mV test pulse for 200 milliseconds revealed fast inactivation when normalized to maximum sodium current.

Recordings of N-type (CaV2.2) voltage-gated calcium currents were obtained using recording solutions and protocols described earlier [58]. The intracellular pipette solution was composed of (in mM): 150 CsCl2, 10 HEPES, 5 Mg-ATP, and 5 BAPTA (pH 7.3, mOsm/L=290–310) and the external solution contained (in mM): 110 NMDG, 10 BaCl2, 30 TEA-Cl, 10 HEPES, 10 glucose and 1 μM TTX (pH 7.3, mOsm/L = ~ 310). To isolate N-type specific calcium currents, the following blockers were used: SNX482 (200 nM, R-type Ca2+ channel blocker), TTA-P2 (1 μM, T-type Ca2+ channel blocker), ω-agatoxin (200 nM, P/Q-type Ca2+ channel blocker), and nifedipine (10 μM, L-type Ca2+ channel blocker). Activation of ICa was measured from a holding voltage of −60 mV for 5 ms followed by 200-ms depolarizing voltage steps from −70 mV to +60 mV in 10-mV increments. Whole-cell currents were normalized to cellular capacitance for analysis of channel activation profiles as a function of voltage in addition to peak current density. Steady-state inactivation of ICa was determined by applying a 1500 ms conditioning prepulse (−100 to +30 mV in +10 mV increments) after which, the voltage was stepped to +10 mV for 200-ms. There were 15-s intervals separating each acquisition to allow channels to revert to their basal state.

2.6 – Preparation of spinal cord slices

Postnatal day 10–14-day rats were deeply anesthetized with isoflurane (4% for induction and 2% for maintaining). For spinal nerve block, 0.3 mL of 2% lidocaine was injected to both sides of L4 to L5 lumbar vertebrae. Laminectomy was performed from mid-thoracic to low lumbar levels, and the spinal cord was quickly removed to cold modified ACSF oxygenated with 95% O2 and 5% CO2. The ACSF for dissection contained the following (in millimolar): 80 NaCl, 2.5 KCl, 1.25 NaH2PO4, 0.5 CaCl2.2H2O, 3.5 MgCl2.6H2O, 25 NaHCO3, 75 Sucrose, 1.3 ascorbate, 3.0 sodium pyruvate with pH at 7.4 and osmolarity at 310 mOsm. Transverse 400 μm thick slices were cut using a vibratome (VT1200S; Leica, Nussloch, Germany). Slices were then incubated for 45 mins at 37°C before a 1h incubation at room temperature (RT) in an oxygenated recording solution containing

the following (in millimolar): 125 NaCl, 2.5 KCl, 1.25 NaH2PO4, 2 CaCl2.2H2O, 1 MgCl2.6H2O, 26 NaHCO3, 25 D-Glucose, 1.3 ascorbate, 3.0 sodium pyruvate with pH at 7.4 and osmolarity at 320 mOsm. The slices were then positioned in a recording chamber and continuously perfused with oxygenated recording solution at a rate of 3 to 4 mL/min before electrophysiological recordings at RT.

2.7 – *Ex-vivo* electrophysiological recordings in spinal cord slices

Substantia Gelatinosa neurons (lamina I/IIo) were visualized and identified in the slices by means of infrared differential interference contrast video microscopy on an upright microscope (FN1; Nikon, Tokyo, Japan) equipped with a 3.40/0.80 water-immersion objective and a charged-coupled device camera. Patch pipettes with resistance at 6 to 10 MΩ were made from borosilicate glass (Sutter Instruments, Novato, CA) on a four-step micropipette puller (P-90; Sutter Instruments, Novato, CA). For spontaneous excitatory postsynaptic current (sEPSC) recordings the pipette solution contained the following (in millimolar): 120 potassium-gluconate, 20 KCl, 2 MgCl2.6H2O, 2.0 Na2-ATP, 0.5 Na-GTP, 20 HEPES, 0.5 EGTA with pH at 7.4 and osmolarity at 310 mOsm. The membrane potential was held at −60 mV using a PATCHMASTER software in combination with a patch clamp amplifier (EPC10; HEKA Elektronik, Lambrecht, Germany).

The whole-cell configuration was obtained in voltage-clamp mode. To record sEPSCs, bicuculline methiodide (10 μM, Cat# 14343, Sigma Aldrich) and strychnine (2 μM, Cat# S0532, Sigma Aldrich) were added to the recording solution to block γ-aminobutyric acid (GABA)-activated and glycine-activated currents. Hyperpolarizing step pulses (5 mV for 50 milliseconds) were periodically delivered to monitor the access resistance (15–25 MΩ), and recordings were discontinued if the access resistance changed by more than 20%. For each neuron, sEPSCs were recorded for a total duration of 2 minutes. Currents were filtered at 3 kHz and digitized at 10kHz. Data were further analyzed by the Mini-Analysis Program (Synaptosoft Inc., NJ) to provide spreadsheets for the generation of cumulative probability plots. The frequency and amplitude of the recordings were compared between neurons from animals in control and in the indicated groups.

2.8 - Immunofluorescence, confocal microscopy, and quantification of CaV2.2 and NaV1.7

Female rat DRG neurons in culture were treated with either PBS (as control), recombinant rat VEGF-A (1 nM), NRP1–4 (12.5 μM), or both NRP1–4 (12.5 μM) + rat VEGF-A (1 nM) for 30 min. Immunofluorescence was performed as described previously[22; 49]. Briefly, cells were fixed for 5 min using ice-cold methanol and allowed to dry at room temperature. Cells were rehydrated in phosphate buffered saline (PBS), and incubated overnight with anti-CaV2.2 antibody (1/200; Cat #: ACC-002, Alomone Labs) or anti-NaV1.7 antibody (1/200; Cat #: MABN41, Sigma-Aldrich) in PBS with 3% bovine serum albumin at 4°C. Cells were then washed 3 times in PBS and incubated with PBS containing 3% bovine serum albumin and secondary antibodies, Alexa 488 goat anti-mouse or Alexa 594 goat anti-rabbit (Thermo Fisher Scientific) for 1 hour at room temperature. After washing with PBS, cells were stained with 49,6-diamidino-2-phenylindole (DAPI, 50 mg/mL) and mounted in ProLong Diamond Antifade Mountant (Cat #: P36961, Life Technologies Corporation). Immunofluorescent micrographs were acquired using a Plan-Apochromat 63x/1.4 oil CS2

objective on a Leica SP8 confocal microscope operated by the LAS X microscope software (Leica). Camera gain and other relevant settings were kept constant throughout imaging sessions. Membrane immunoreactivity was calculated by measuring the signal intensity in the area contiguous to the boundary of the cell. The membrane to cytosol ratio was determined by defining regions of interest in the cytosol and on the membrane of each cell using Image J. Total fluorescence was normalized to the area analyzed and before calculating the ratios.

2.9 – National Institute of Mental Health's Psychoactive Drug Screening program (NIMH PDSP) radioligand binding assays

NRP1–4 was tested at a single concentration (10 μM) in quadruplicate by the PDSP in primary binding assays as described previously [4]. The PDSP database automatically marks those entries with 50% or higher inhibition for secondary binding assays and highlights those with variances greater than 20% among the quadruplicate determinations for further inspection. Secondary radioligand binding assays determine equilibrium binding affinity for the specific targets selected.

2.10 – NIMH PDSP GPCRome assay

NRP1–4 was submitted to the PDSP GPCRome screening, via a variation of the transcriptional activation following arrestin translocation (TANGO) assay described in [41]. The Parallel Receptor-ome Expression and Screening via Transcriptional Output-TANGO (PRESTO-TANGO) assay screens collections of molecules against the entire human druggable GPCR-ome. Activation of the D2 GPCR by 100 nM of the D2R agonist quinpirole is used as a positive control. The results are reported as fold change of average basal responses and potential targets are those with responses falling above the >3-fold cutoff.

2.11 – Intrathecal catheter implantation in adult rats

For intrathecal (i.t.) drug administration, rats were chronically implanted with catheters as described by Yaksh and Rudy [69]. Briefly, rats were anesthetized using isoflurane (4% for induction and 2% for maintaining) and placed in a stereotaxic head holder. The cisterna magna was exposed and incised, and an 8-cm catheter (PE-10; Stoelting) was implanted, terminating in the lumbar region of the spinal cord. Catheters were sutured (3–0 silk suture) into the deep muscle and externalized at the back of the neck; skin was closed with autoclips. After a recovery period of 5–7 days after implantation of the indwelling cannula, the spared nerve injury was induced.

2.12 – Spared Nerve Injury (SNI) model of neuropathic pain

The neuropathic pain model induced by spared nerve injury (SNI) in rats was obtained as previously described [50]. Adult male rats (250g, Envigo) were anesthetized with isoflurane (5% induction, 2.0% maintenance in 2 L/min air), and skin on the lateral surface of the left hind thigh was incised. Then, the biceps femoris muscle was dissected to expose the three terminal branches of the sciatic nerve. the common peroneal and tibial branches were tightly ligated with 4–0 silk and axotomized 2.0 mm distal to the ligation. Sham animals underwent

the same operation, but the exposed nerves were not ligated. Closure of the incision was made in two layers. The muscle was sutured once with 5–0 absorbable suture; skin was autoclipped. Animals were allowed to recover for 7 days before any testing. Mechanical allodynia was assessed 10 days after surgery as previously described [50] using Von Frey filaments. Briefly, rats were allowed to acclimate within suspended wire mesh cages for 30 min prior to behavioral assessment. Before (Baseline), after SNI (Pre-drug) and 30, 60, 120, 180, 240, 300 minutes post-i.t. time points were used to measure response to calibrated von Frey filaments (g) applied perpendicular to the lateral plantar surface of the left hind paw (up-down method). Paw withdrawal thresholds were calculated in grams using the Dixon non-parametric test and expressed as the Paw Withdrawal Threshold (mean ± standard error; SEM) in GraphPad Prism 9.0. All behavior experiments were blinded.

2.13 – Intravenous (i.v.) administration of NRP1–4

For i.v. administration, rats were mechanically restrained using a fabric cloth, allowing easy access the tail. Rat tails were wiped with 2% chlorhexidine, and NRP1–4 (20 μg, 200 μL, first dissolved in DMSO then in saline) or vehicle (1% DMSO in saline, 200 μL) were injected in one of the lateral tail veins using 1 mL syringes (23-G needles). Correct placement of the needle was verified by a gentle aspiration to confirm blood flow. Following injection, the experimenter applied gentle pressure with a gauze until bleeding has stopped.

2.14 – L5/L6 Spinal Nerve Ligation (SNL) model of neuropathic pain

L5/L6 spinal nerve ligation (SNL) induces tactile allodynia and thermal hypersensitivity. For SNL, surgeries were done as previously described [38]. Rats were anesthetized with 2% isoflurane in O2 anesthesia (total time under anesthesia was < 30 minutes). The skin over the caudal lumbar region was incised and the muscles retracted. The L5 and L6 spinal nerves were exposed, carefully isolated, and tightly ligated with 4–0 silk distal to the dorsal root ganglion without limiting the use of the left hind paw of the animal. All animals were allowed 14 days to recover before any behavioral testing. Any animals exhibiting signs of motor deficiency were euthanized. Sham control rats underwent the same operation and handling as the SNL animals, but without the nerve ligation.

2.15 – Measurement of thermal sensory thresholds

Hargreaves' test: for rats, paw withdrawal latencies were determined as described by Hargreaves et al. [32]. Briefly, rats were acclimated within Plexiglas enclosures on a clear glass plate at least for 15 minutes. A radiant heat source (high-intensity projector lamp) was focused onto the plantar surface of the hind paw. Withdrawal latencies were measured using a motion detector that halted the stimulus and a timer. A maximal cutoff of 33.9 sec was used to prevent tissue damage.

2.16 – Measurement of tactile sensory thresholds

The assessment of tactile sensory thresholds was determined by measuring the withdrawal response to probing the plantar surface of the hind paw with a series of calibrated fine filaments (von Frey). Each filament was applied perpendicularly to the plantar surface of the paw of rats and mice held in suspended wire mesh cages. The "up and down" method

was used to identify the mechanical force required for a paw withdrawal response. Data were analyzed with the nonparametric method of Dixon, as described by Chaplan et al. [10]. Results are expressed as the mean withdrawal threshold that induces a paw withdrawal response in 50% of animals.

2.17 – Algogram assay for assessment of nociceptive behaviors and toxicity

Adult male rats were tested using a battery of behavioral methods [28] to screen the antinociceptive effects of treatment with NRP1–4, which was delivered via the intrathecal route. The following behavioral assays were performed: paw pressure test [59], tail flick test [1; 42], acetic acid-induced abdominal cramping [31], formalin test [21], Bennett model of peripheral neuropathy [3], oxaliplatin-induced neuropathy [11], carrageenan-induced pain [59], effects of kaolin on gait [53], the Brennan model of postoperative pain [7], and TNBS induced colonic distension [20]. In the Brennan model for evaluation of incisional pain, 24 hours after surgery electronic von Frey was used to determine sensory thresholds [10]. In addition to the pain behaviors outlined above, the animals were also tested in the Irwin grid, which is part of a common core of tests used to evaluate the safety and toxicity of new compounds [60]. This test includes ranking 38 standard parameters (e.g., eating, drinking, defecation, respiration, heart rate, etc.) that are assessed in the home cage environment, an open arena, and a contested environment. Changes to these parameters provide insight as to whether the normal neurophysiological function of the animal has been impaired by the treatment. These behavioral tests were performed using a high throughput screening approach with 4 rats per sample group and this was repeated twice for a total of 8 rats per condition. Measured outputs (e.g., withdrawal thresholds or reaction times) were normalized to internal controls or within subject controls, such as to the contralateral uninjured paw. This approach allowed for the screening of NRP1–4 for identification of off-target effects on normal sensory function as well as a variety of pain modalities.

2.18 – Statistical methods and data analysis

Graphing and statistical analysis were undertaken with GraphPad Prism Version 9 (San Diego, California). Representative trace waveforms were generated using OriginPro Version 2022. I-V curve fitting was performed using the Fitmaster software package from HEKA Elektronik to determine the reversal potential and conductance parameters. All data sets were tested for normality using D'Agostino & Pearson test. Details of statistical tests, significance and sample sizes are reported in the appropriate figure legends. All data plotted represent mean ± SEM. For electrophysiological recordings: peak current density was compared using Mann-Whitney tests, One-way ANOVA with the Tukey post hoc test and Kruskal–Wallis test with Dunnett's post hoc comparisons; $V_{1/2}$ midpoint potential and k slope factor, were analyzed with Mann-Whitney test and one-way ANOVA with Tukey post hoc test. Statistical significance of thermal sensitivity was compared by the Kruskal-Wallis test followed by the Dunn post hoc test. Behavioral data with a time course were analyzed by two-way ANOVA and area under the curve (AUC) was analyzed using the Kruskal-Wallis test. All behavioral tests were performed by an experimenter blind to the treatment condition and analysis was performed before unblinding occurred. Full details of statistical analyses for all figures can be found in table S1.

3.0 – Results

3.1 – Discovery of small molecule inhibitor of NRP1/VEGF-A interaction

NRP-1 is a modular protein with a single transmembrane helix, three extracellular domains, and a cytoplasmic tail region (Figure 1A), reviewed in [29]. To target the interaction between VEGF-A and NRP-1, we previously conducted a virtual screen against the VEGF-A binding pocket on the NRP-1 b1 domain. We then evaluated hit compounds for their ability to suppress VEGF-A/NRP1 coupling and phosphorylation of VEGFR2's cytoplasmic domain at tyrosine residue 1175 (Y1175) — a surrogate measure of the activation of the VEGFA pathway [55]. We found that six compounds disrupted binding of VEGF-A to NRP1 more effectively than the commercially available NRP-1 inhibitor EG00229 [55]. The docked pose of the lead compound from this series, 4'-methyl-2'-morpholino-2-(phenylamino)-[4,5'-bipyrimidin]-6(1H)-one, (designated herein as NRP1–4) predicts interactions with key NRP1 residues responsible for stabilizing the interaction with VEGF-A, including T349, and Y353 [29; 55] (Figure 1B, C). NRP1–4 inhibited the NRP1/VEGF-A interaction with an IC_{50} of 0.598 nM compared to an IC_{50} of 930 nM for EG00229 in a cell-free assay [55]. These findings suggested that NRP1–4 could serve as a lead compound for investigation of signaling pathways downstream of NRP1 activation, as well as efficacy in preclinical models of chronic pain.

3.2 – NRP1–4 blocks VEGF-A-induced increase in DRG excitability

The excitability of primary afferent neurons is the ultimate determining factor for conveying nociceptive information from the periphery to the central nervous system. If VEGF-A increases neuronal excitability of primary afferent neurons, then this would support our model where VEGF-A serves as a pro-nociceptive factor. To test this question, we isolated primary sensory neurons and elicited action potential firing from these cells by injecting depolarizing current into the soma in a stepwise manner. We first began by eliciting action potentials from neurons that were completely untreated to determine what the baseline level of excitability in this preparation (Figure 2A, gray trace). We then treated the primary sensory neurons with vehicle control (DMSO), VEGF-A, NRP1–4, and VEGF-A + NRP1–4 (Figure 2A, B). We then quantified the number of action potentials fired at the 60pA current step and found that VEGF-A significantly enhanced action potential firing compared to the control condition (DMSO vs. VEGFA P=0.0157, Figure 2C and Table S1). Since our modeling studies showed that NRP1–4 occupies the site of NRP1 where VEGF-A binds, we then wondered whether NRP1–4 could then block this pro-nociceptive increase in neuronal excitability. Consistent with our previous work and computational results the enhancement in neuronal excitability induced by VEGF-A was completely blocked by treatment with NRP1–4 (VEGFA vs. NRP1–4 + VEGFA P=0.0390, Figure 2C and Table S1). While it appears that there was an effect of NRP1–4 on action potential firing, this difference was not significant (DMSO vs. NRP1–4 P=0.1824, Figure 2C and Table S1). In addition, we found that the DMSO group was identical to the group with no drug in the external solution, indicating that the DMSO did not affect the electrophysiological properties of our sensory neuron system (Drug Free vs. DMSO P>0.9999, Figure 2 and Table S1). In addition to the excitability parameters, we also measured the rheobase, which is the current required to fire a single action potential. Treatment with VEGF-A significantly reduced the rheobase

compared to vehicle treated control (DMSO vs. VEGFA P=0.0310, Figure 2D and Table S1). Co-treatment with NRP1–4 blocked the effect of VEGF-A on rheobase in DRG sensory neurons (VEGFA vs. NRP1–4 + VEGFA P=0.0114, Figure 2D and Table S1). There was no effect of any of the treatments on the basal resting membrane potential levels (Figure 2E and Table S1). From these results we can conclude that VEGF-A significantly potentiates neuronal excitability in primary sensory neurons and that this enhancement can be blocked by co-treatment with NRP1–4. This suggests that NRP1–4 interferes with the action of VEGF-A at its receptor in complex with NRP1 on the surface of sensory neurons.

3.3 – NRP1–4 attenuates VEGF-A mediated increases in sodium currents

We previously found that VEGF-A increased both sodium and N-type calcium currents in DRG neurons [51]. Therefore, we first tested if NRP1–4 could block VEGF-A mediated sodium current increase in cultured primary sensory neurons isolated from female rats (Figure 3A). Using stepwise depolarizing pulses, we interrogated the activation and inactivation properties of the voltage-gated sodium channel populations in these neurons (Figure 3B). Treatment of DRG neurons with VEGF-A resulted in increased sodium currents elicited by successive depolarizing pulses (Figure 3C). NRP1–4 prevented this VEGF-A mediated increase in sodium current (Figure 3C–D and Table S1). The increased sodium current density by VEGF-A treatment, was blocked by co-application of NRP1–4 (VEGF-A vs. VEGF-A + NRP1–4, P=0.0152, Figure 3E and Table S1). There was no difference in voltage-dependent activation or inactivation observed between any of the groups (Figure 3F and Table S2). These results confirm our previous report that VEGF-A potentiates sodium currents in DRG neurons responsible for transmission of nociceptive information. Importantly, treatment with NRP1–4, which binds to the VEGF-A pocket of the b1 domain of NRP1, significantly blocked the potentiating effects of VEGF-A. Treatment with NRP1–4 alone had no effect on sodium currents in DRG neurons, which shows that the prevention of sodium current density increase, is indeed due to blockade of VEGF-A.

3.4 – Inhibition of VEGF-A mediated increase in sodium currents by NRP1–4 is through NaV1.7

The excitability of peripheral sensory neurons is determined largely by the expression of voltage-gated ion channels, including sodium and calcium channels, in the plasma membrane. There are several voltage-gated sodium channels expressed in peripheral sensory neurons of the DRG. Of those expressed in the DRG, the voltage-gated sodium channel isoform 1.7 (NaV1.7) has a significant role in the initiation of action potentials [19; 43]. As we observed increased sodium current density in DRG neurons following treatment with VEGF-A, which was blocked by co-treatment with NRP1–4, we were curious whether NaV1.7 might be responsible for this effect. To determine this, we used the highly selective NaV1.7 peptide blocker Protox-II (PrTx-II), which has significantly higher affinity for NaV1.7 over other sodium channel isoforms [62]. We then recorded sodium currents from DRG neurons and found that treatment with VEGF-A potentiated sodium currents, as was observed previously (Figure 3A). We used the same series of stepwise depolarizing pulses to interrogate the sodium current activation and inactivation properties as used above (Figure 4B). Co-treatment of DRG neurons with VEGF-A significantly enhanced sodium current density in cultured DRG neurons (Vehicle vs. VEGF-A P=0.0160, Figure 4C&D

and Table S1). Co-application of the NaV1.7 inhibitor PrTx-II abolished the potentiation that was previously observed by VEGF-A (VEGF-A vs. VEGF-A + PrTx-II P=0.0192, Figure 4C&D and Table S1). As observed above, NRP1–4 blocked the effect of VEGF-A and co-application of PrTx-II did not produce a further reduction in peak sodium current density (VEGF-A vs. NRP1–4 + VEGF-A P=0.0398; NRP1–4 + VEGF-A vs. NRP1–4 + VEGF-A + PrTx-II P>0.9999, Figure 4D and Table S1). Application of PrTx-II and VEGF-A caused a shift in the half maximal activation voltage when compared to VEGF-A alone (VEGF-A vs. VEGF-A + PrTx-II P=0.0220, Figure 4E and Table S2). Additionally, the half maximal inactivation voltage of the VEGF-A + PrTx-II group was significantly different than the half-maximal voltage of the VEGF-A group alone (VEGF-A vs. VEGF-A + PrTx-II P=0.0274, Figure 4E and Table S2). These effects are consistent with the mechanism of action for PrTx-II since this peptide targets the voltage sensing region of NaV1.7 [62; 68]. Together, these findings demonstrate that the increase in sodium current density observed upon application of VEGF-A is mediated completely by NaV1.7, since this increase was blocked fully by PrTx-II.

3.5 – NRP1–4 reverses VEGF-A mediated increase in N-type calcium currents

In addition to voltage-gated sodium channels, voltage-gated calcium channels are also critical regulators of excitability of primary afferent neurons. Specifically, the N-type voltage-gated calcium channel has been implicated in the transmission of nociceptive signals from the periphery to the CNS due to its expression on presynaptic terminals from the DRG to the spinal cord. Since N-type channels are crucial mediators of excitability we next tested if NRP1–4 could prevent the VEGF-A mediated potentiation of N-type currents in DRG neurons. We isolated N-type currents from small-diameter sensory neurons using a solution containing specific blockers of other voltage-gated calcium channel subtypes (Figure 5A). We then subjected these neurons to a series of protocols to evaluate their activation and steady-state fast inactivation properties in the presence of VEGF-A and NRP1–4 (Figure 5B). Treatment with VEGF-A potentiated calcium currents through CaV2.2 channels in sensory neurons, which was blocked by NRP1–4 (Figure 5C–D and Table S1). VEGF-A-mediated increase in N-type calcium current density was prevented by co-application of NRP1–4 (Vehicle vs. VEGF-A, P = 0.0032; Vehicle vs. NRP1–4, P>0.9999; NRP1–4 vs. VEGF-A + NRP1–4, P>0.9999; Figure 5E and Table S1). NRP1–4 had no effect when applied alone. There was no change observed in the voltage-dependent activation or steady-state fast inactivation across any of the conditions (Figure 5F and Table S2). These results show that NRP1–4 abolished the increase of N-type calcium currents induced by treatment with VEGF-A.

3.6 – NRP1–4 reverses VEGF-A mediated surface expression of CaV2.2 and NaV1.7

The findings above show that VEGF-A increased NaV1.7 and CaV2.2 current density in primary sensory neurons, which could be blocked by co-application of NRP1–4, while not affecting the biophysical properties of these channels. This suggested that the changes we observed were due to differences in the expression of these channels in the sensory neuronal plasma membrane. To determine whether VEGF-A enhanced NaV1.7 and CaV2.2 membrane expression, and whether this could be blocked by NRP1–4, we used immunofluorescent labeling followed by confocal imaging to visualize the expression

of both CaV2.2 and NaV1.7 in cultured rat DRG sensory neurons (Figure 6A). When quantifying the fluorescent intensity under these treatment conditions we found that VEGF-A significantly enhanced the expression of CaV2.2 compared to control (Vehicle vs. VEGFA P=0.0352, Figure 6B and Table S1). This VEGF-A mediated increase in CaV2.2 expression was prevented by co-treatment with NRP1–4 (VEGFA vs. NRP1–4 + VEGFA P<0.0001, Figure 6B and Table S1). When probing the expression of NaV1.7 we also found that the normalized surface expression of this channel was increased by VEGF-A (Vehicle vs. VEGFA P=0.0037, Figure 6C and Table S1). Additionally, the increased expression as a result of VEGF-A was blocked by co-treatment with NRP1–4 (VEGFA vs. NRP1–4 + VEGFA P=0.0380, Figure 6C and Table S1). When combined with our findings using patch clamp electrophysiology, these results suggest that the expression of NaV1.7 and CaV2.2 is enhanced by VEGF-A and that this enhancement is blocked by co-treatment with NRP1–4.

3.7 – Treatment with NRP1–4 blocks VEGFA–mediated increase in synaptic activity

The above and published results show that VEGF-A sensitizes electrogenesis (dependent on sodium channels) and neurotransmitter release (regulated by N-type calcium channel) [51]. Because these parameters ultimately control spinal nociceptive neurotransmission, we then tested whether NRP1–4 could also act on VEGF-A induced enhancement of spinal synaptic transmission. We performed electrophysiological recordings in spinal cord slices obtained from young rats. Specifically, we measured spontaneous excitatory post synaptic currents (sEPSCs) in neurons of the *substantia gelatinosa* region of the lumbar dorsal horn, which includes the outer laminae that are targets for nociceptive primary sensory projections. Acute perfusion with VEGF-A (4 nM) in the external bath solution increased sEPSC frequency compared with control slices (1.760 ± 0384 Hz [VEGF-A] vs 0.703 ± 0.113 Hz [Control], P = 0.0051, Figure 7A–B and Table S1). Interestingly, addition of VEGF-A also increased sEPSC amplitude (26.59 ± 1.541 pA [VEGF-A] vs 19.76 ± 1.315 pA [Control], P = 0.0031, Figure 7A and C and Table S1). However, when VEGF-A was co-applied with NRP1–4 (12.5 μM), the potentiating effect of VEGF-A was nullified. Both sEPSC frequency (0.843 ± 0.157 Hz [VEGFA + NRP1–4] vs 1.760 ± 0.384 Hz [VEGF-A], P = 0.0439, Figure 7B and Table S1) and amplitude (19.73 ± 1.236 pA [VEGF-A + NRP1–4] vs 26.59 ± 1.541 pA [VEGF-A], P = 0.0082, Figure 7C and Table S1) were lower when the slices were perfused with both VEGF-A and NRP1–4 compared to VEGF-A alone. Acute perfusion of the NRP1–4 alone did not change the frequency (P = 0.5259, Figure 7B and Table S1) or the amplitude (P = 0.9799, Figure 7C and Table S1) of sEPSCs compared with the vehicle control, showing no intrinsic effect of NRP1–4 on basal excitatory tone in nociceptive synapses of the lumbar dorsal horn. Together, these results corroborate our previous findings with EG00229 and Spike protein [51], clearly demonstrating that interfering with NRP1 activation by blocking binding of VEGF-A normalizes potentiated signaling in the spinal cord [51].

3.8 – NRP1–4 selectivity profile

Since NRP1–4 reduces calcium and sodium currents through binding to NRP1 and inhibits the effects of VEGF-A, it is possible that NRP1–4 could also bind to other receptors expressed in sensory neurons. To screen for potential off-target liabilities as a result of binding to receptors and transporters, NRP1–4 was subjected to a rigorous pharmacological

screening campaign through the National Institute of Mental Health's Psychoactive Drug Screening Program (NIMH PDSP) [4]. The radioligand binding assays test nonspecific binding to 46 different transporters including norepinephrine transporter (NET), serotonin transporter (SERT), and receptors such as histamine, dopamine, serotonin, muscarinic, adrenergic, and opioid receptors. Interestingly, we found that NRP1–4 binds to the serotonin 5-HT7A receptor, and histamine H1 receptor (Table S3). While NRP1–4 did bind to these two targets, the dissociation constant is relatively high compared to the interaction between NRP1–4 and its intended target NRP1/VEGF-R2 (0.598 nM).

As a subset of the PDSP screen, we also performed a screen against ~300 GPCR targets expressed in humans. This screening tool is known as the GPCRome [41] and it uses a variation of the transcriptional activation following arrestin translocation (TANGO) assay to screen for molecules against the druggable human GPCR-ome, including the opioid receptors. Results demonstrated that NRP1–4 is a potential activator of G-coupled receptors encoded by the following human genes: ADRA2A (adrenoreceptor alpha 2A), ADRA2B (adrenoreceptor alpha 2B), GPRC5D (G-protein coupled receptor family C group 5 member D), and ADORA1 (adenosine A1) (Table S4). However, no activation of the μ (MOR), δ (DOR), or κ (KOR) opioid receptors was detected. These results show that NRP1–4 does not have off-target liability at any of the human opioid receptors.

3.9 – Central administration of NRP1–4 reverses SNI-induced mechanical allodynia in rats

Treatment with NRP1–4 produced reversal of VEGF-A induced enhancement of sEPSC amplitude and frequency in the spinal cord and reduced currents through pain-relevant voltage-gated ion channels in primary afferent neurons. Based on these findings, we next asked if NRP1–4 treatment could affect pain behavior in a rodent model of chronic pain. We tested this question *in vivo* using the SNI model of neuropathic pain (Figure 8A). We previously showed that there was no sex difference in VEGF-A mediated mechanical and thermal hypersensitivity and chose to use only male rats for the next experiments. SNI resulted in increased plantar sensitivity on the ipsilateral side relative to the injury (Figure 8). On the day of testing, NRP1–4 was intrathecally (i.t.) delivered through a spinal cannula extending to the lumbar level and paw withdrawal thresholds were then recorded every hour for 5 hours (Figure 8B). Rats treated with NRP1–4 demonstrated a significant reversal in mechanical allodynia 60 minutes post-injection ($P=0.0119$, Figure 8C and Table S1) that was maintained for the 2 ($P<0.0001$, Figure 8C and Table S1) and 3 ($P<0.0001$, Figure 8C and Table S1) hour post-injection time points. We used the area bounded by the curves in Figure 8B and the x-axis to determine the area under the curve. When this value was plotted, we found that paw withdrawal thresholds were significantly higher for the group treated with NRP1–4 when compared to the saline-treated control (AUC: 33.26 ± 6.125 [NRP1–4] vs 4.351 ± 1.123 [Control], $P = 0.0159$, Figure 8D and Table S1). This shows that, in addition to reversing mechanical allodynia at specific time points, the mechanical sensitivity over time was reversed for animals treated with NRP1–4, indicating relief of previously present mechanical allodynia. These findings were consistent with our previous results using EG00229 or Spike protein [51] and support the conclusion that blocking the interaction of VEGF-A with NRP1 following central administration of NRP1–4 is sufficient to reverse experimental neuropathic pain induced by spared nerve injury in rats.

To expand upon this initial finding with nerve injury and investigate the effects of NRP1–4 on nociceptive behaviors, as well as to evaluate potential toxicity, we performed a battery of high throughput behavioral tests. This approach allows for screening novel compounds in a variety of assays that evaluate treatment efficacy in models of visceral pain, inflammatory pain, neuropathic pain, chemotherapy-induced pain, post-surgical pain, and in physiological nociception (see methods). Using this technique, we found that NRP1–4 does not produce overt toxicity, as evidenced by the fact that there was no change in the physiological state of the animals measured using the Irwin grid assay (Table S5). Treatment with NRP1–4 reduced mechanical allodynia following injection with carrageenan, reduced the time spent licking the paw in the formalin test, and reduced the number of abdominal cramps in the acetic acid test (Figure S1). Together with the effects observed in SNI rats, these findings suggest that NRP1–4 could be a useful tool in neuropathic pain, as well as inflammatory or visceral pain conditions.

3.10 – Intravenous administration of NRP1–4 reverses mechanical allodynia and thermal hyperalgesia in male rats

Since central delivery of pain therapies is often not feasible and can be associated with negative treatment-associated outcomes, such as infection, we explored intravenous (i.v.) injection for systemic delivery of NRP1–4. In addition, we employed another model, spinal nerve ligation (SNL), to complement our findings above with the spared nerve injury model. We found that in animals with sham surgery, NRP1–4 had no effect on mechanical withdrawal thresholds following i.v. injection (Figure 9A and Table S1). In rats with SNL-induced nerve injury, there was a significant reduction in paw withdrawal threshold, which was maintained for the entire duration of the experimental window (Figure 9A and Table S1). Treatment with NRP1–4 (20 μg) reversed experimental neuropathic pain induced by SNL, at the 0.5 ($P<0.0001$ SNL NRP1–4 vs SNL Vehicle, Figure 6A), 1 hour ($P<0.0001$ SNL NRP1–4 vs SNL Vehicle, Figure 9A and Table S1), and 2-hour ($P<0.0001$ SNL NRP1–4 vs SNL Vehicle, Figure 9A and Table S1) time points following i.v. administration. Quantification of this effect by calculating the area bounded between these curves and the x-axis demonstrated a significant difference between the sham and SNL-Vehicle groups ($P<0.0001$, Figure 9B and Table S1). Treatment with NRP1–4 reversed mechanical allodynia compared to the SNL-Vehicle group ($P=0.0558$, Figure 9B and Table S1). In addition to mechanical withdrawal thresholds, we also evaluated thermal withdrawal latency, a measure of thermal hyperalgesia, using the Hargreaves assay. Animals with sham surgery and NRP1–4 administration did not display significant deviation from baseline following injection of the compound intravenously (Figure 9C and Table S1). Those animals with spinal nerve ligation and vehicle treatment displayed significant hyperalgesia, as demonstrated by their reduced latency to withdraw from an aversive thermal stimulus (Figure 9C and Table S1). Treatment with NRP1–4 reversed this decreased latency at the 0.5 ($P=0.0011$, Figure 9C), the 1-hour ($P=0.0135$, Figure 9C and Table S1), and 2-hour ($P=0.0001$, Figure 9C and Table S1) time points. When we quantified this difference using the area bounded by the curve and the x-axis (area under the curve), we observed that the animals with nerve injury and saline treatment had significantly decreased withdrawal latency ($P<0.0001$, Figure 9D and Table S1). Intravenous injection with 20 μg of NRP1–4 significantly reversed this trend and increased the withdrawal latency ($P=0.0459$, Figure 9D and Table S1). Together, these

findings complement the results from our studies with animals with spared nerve injury and show that treatment with NRP1–4, when given systemically, can reverse the symptoms of mechanical allodynia and thermal hyperalgesia associated with nerve injury-induced pain.

4.0 – Discussion and Conclusion

Few treatments available are available for chronic pain that are both safe and efficacious. As part of the etiology of chronic pain, many endogenous mediators can trigger sensitization of neurons within the nociceptive sensory pathways that enhances pain transmission. One such mediator is VEGF-A which signals through membrane-bound tyrosine kinase receptors, including VEGF-Rs and co-receptors including Neuropilin-1 (NRP1). Clinical evidence supports a role for VEGF-A in nociception: patients with osteoarthritis have increased VEGF levels in their synovial fluid, which correlates with higher pain scores [64]. There have also been reports linking VEGF signaling with diverse pain syndromes including pelvic pain, cancer-induced bone pain, and chemotherapy-induced peripheral neuropathy [18; 24; 27]. These reports suggest that VEGF could be a common component of pain disorders with varying etiologies, which suggests that VEGF signaling is likely complex and could serve as the foundation for novel pain therapeutics.

Our results expand upon the role of VEGF-A in mediating nociceptive neurotransmission and implicate its co-receptor, Neuropilin-1, as a novel target for interfering with VEGF-A mediated pro-nociception. Here we have shown that disrupting the binding between VEGF-A and NRP1 (i) decreases sensory neuron excitability (ii) decreases surface expression and function of NaV1.7 and Cav2.2 in DRGs; (iii) decreases nociceptive spinal neurotransmission; and (iv) reverses experimental neuropathic pain in two different preclinical pain models without causing toxicity (Figure 5, 6). These findings are consistent with the previously validated role of the VEGF-A signaling pathway in modulating neurotransmission and synaptic strength [45]. Previous studies reported that VEGF-A levels are increased following spinal cord injury and that this increase is directly correlated with the development of mechanical allodynia [52]. In addition, VEGF-A release directly modulates ion channel function and causes increased intracellular calcium flux [40; 46]. These lines of evidence support the notion that VEGF-A, through its activity at the NRP1/VEGF-R2 complex, increases depolarizing currents in sensory neurons, which leads to enhanced pain sensations. This is consistent with our own observation that VEGF-A enhances excitability and decreases rheobase in sensory neurons, which is prevented by co-application of NRP1–4. We conclude that treatment with NRP1–4, which we have previously shown decreases VEGF-R2 phosphorylation, interferes with this potentiating effect of VEGF-A and acts to suppress the development of neuropathic pain [55].

Our findings are consistent with previous work interrogating NRP1 signaling using either recombinant Spike protein, derived from the capsid of SARS-CoV-2, or EG00229 – a commercially available NRP1 antagonist [51]. We modeled the chemical properties of Spike protein and EG00229 as a scaffold for the identification of a pharmacophore targeting the VEGF-A/NRP1 interaction, which then spurred the discovery of several compound series, and ultimately yielded the NRP1 inhibitor NRP1–4 [55]. Both Spike protein and EG00229 have poor pharmacokinetic properties, suffering from high hydrophobic surface area, in the

case of Spike protein, and poor tissue penetration in the case of EG00229. Our compound, NRP1–4 was predicted to have favorable pharmacokinetic properties, which is supported by the finding that systemic administration of NRP1–4 (i.v., Figure 6) mimicked central administration (i.t., Figure 5), suggesting that this compound penetrates tissue barriers to reach its target. We conclude that NRP1–4 has significant potential as an analgesic candidate, since it is both stable and soluble enough to survive systemic biodistribution.

While NRP1–4 is quite effective in reducing pain, some of the data we reported here points toward other interactions that need to be further explored. For example, in the binding assays and GPCRome screen for off-target activity several 'hits' were identified, including binding to the serotonin receptor 5-HT7A and the histamine receptor H1. It is possible that these interactions indicate side effects that need to be investigated when developing NRP1–4 as a drug candidate. However, it is unlikely that the interactions with the serotonin receptor or the histamine receptor are of significant concern. This is because the Ki for these interactions is in the micromolar range, whereas the IC_{50} for NRP1–4 at NRP1 is far below this level, in the sub-nanomolar range (0.598 nM) [55]. This means that the doses needed to achieve analgesic efficacy are unlikely to rise to the levels necessary to activate off-target interactions. Additionally, the interactions identified by the GPCRome screen are also unlikely to cause concern because three of the four interactions were very close to the detection threshold (GPRC5D, ADRA2A, and ADORA1). The only interaction that was significantly above the detection limit was ADRA2B, which is the gene encoding the alpha-2β adrenergic receptor and is involved in neurotransmitter release within the sympathetic nervous system. Dysregulation of sympathetic innervation, in the form of sympathetic sprouting and the formation of baskets around sensory neurons, is a phenomenon observed in models of neuropathic pain [57]. Since NRP1–4 potently reverses neuropathic pain, its suppression of sympathetic GPCR function could potentially be an additional factor mediating the analgesic efficacy observed in our studies.

In addition to its role in bone cancer pain, there have also been reports of involvement of VEGF-A in diverse pain syndromes including rheumatoid arthritis, osteoarthritis, and chemotherapy-induced peripheral neuropathy [30]. Moreover, VEGF-A is intimately involved in the vascularization of cancerous tumors, which has led to the development of potent antibodies targeting this receptor. A recent report demonstrated that paclitaxel-induced peripheral neuropathy could be reversed following administration of a monoclonal antibody targeting VEGF-A [47]. This finding supports our observation that VEGF-A is pro-nociceptive and that blocking its effects on nociceptive neurons can produce anti-nociception. While using a monoclonal antibody produces specificity for a target, VEGF-A has effects throughout the body and global depletion of VEGF-A levels would not be advisable in the setting of chronic pain. Our approach utilizes an alternative strategy to achieve specificity, by targeting the VEGF-A co-receptor, NRP1, which co-localizes with VEGF-A in a narrow range of tissues, which includes nociceptive sensory neurons. Since NRP1–4 was optimized for the VEGF-A binding pocket in the b1 domain of NRP1, administration of this inhibitor will only block the pro-nociceptive effects of VEGF-A in tissues where VEGF-R2 co-localizes with NRP1, such as in sensory neurons. However, because NRP1 is expressed on blood vessels, it is possible that targeting this receptor could result in some vascular complications. To address this possibility, we investigated

potential off target toxicity using the Irwin grid, which evaluates respiratory rate, heart rate, body temperature, and muscle tone, among other somatic factors indicative of vascular complications (Table S5, Figure S1). This assay did not reveal any systemic toxicity due to NRP1–4 administration and suggests that NRP1–4 does not produce adverse vascular complications, which further supports our selective targeting strategy.

In addition to the positive outcomes reported in our results above, there are some limitations of our approach that need to be considered when interpreting the findings from this study. A limitation of our study is that our DRG recordings included nerve growth factor (NGF) in the culture media, this might be affecting VEGF-A concentration since it has been reported that application of NGF increases VEGFA mRNA expression in non-neuronal cells [37; 48; 66]. Also, both growth factors have been implicated in angiogenic and neurotrophic effects, leaving open the possibility of a crosstalk between the signaling cascades and their potential activation of the ERK pathway. One way to overcome this would be to dissect the role of NGF and VEGF-A in nociceptors, and the signaling cascades they activate, using small molecules that specifically inhibit each receptors' activity.

In conclusion, we have shown that NRP1–4 is a novel inhibitor of NaV1.7 and N-type calcium channels that reduces neuronal excitability and reverses experimental neuropathic pain. Additionally, we have shown there are limited off-target effects at human GPCR's and there was no toxicity observed when screening NRP1–4 in rats. Our studies have demonstrated that this compound targets NRP1 and it therefore has the potential to serve as a lead compound development of a novel analgesic class targeting the NRP1/VEGF-R2 complex.

Supplementary Material

Refer to Web version on PubMed Central for supplementary material.

Acknowledgements –

This study was supported by NIH awards from NINDS (NS098772, NS120663, and NS122545 to R.K.) and NIDA (DA042852 to R.K.). R.K. is the founder of Regulonix LLC, a company developing nonopioid drugs for chronic pain. In addition, R.K., has patents US10287334 (non-narcotic CRMP2 peptides targeting sodium channels for chronic pain) and US10441586 (SUMOylation inhibitors and uses thereof) issued to Regulonix LLC. The other authors declare that they have no competing interests. R.K. and A.M are cofounders of EleutheriaTx Inc., a company developing gene therapy approaches for chronic pain. Receptor binding profiles and GPCRome data was generously provided by the National Institute of Mental Health's Psychoactive Drug Screening Program, Contract # HHSN-271-2018-00023-C (NIMH PDSP). The NIMH PDSP is Directed by Bryan L. Roth MD, PhD at the University of North Carolina at Chapel Hill and Project Officer Jamie Driscoll at NIMH, Bethesda MD, USA.

References

[1]. Amour FE, Smith DL. A METHOD FOR DETERMINING LOSS OF PAIN SENSATION. Journal of Pharmacology and Experimental Therapeutics 1941;72(1):74.

[2]. Basbaum AI, Bautista DM, Scherrer G, Julius D. Cellular and molecular mechanisms of pain. Cell 2009;139(2):267–284. [PubMed: 19837031]

[3]. Bennett GJ, Xie YK. A peripheral mononeuropathy in rat that produces disorders of pain sensation like those seen in man. Pain 1988;33(1):87–107. [PubMed: 2837713]

[4]. Besnard J, Ruda GF, Setola V, Abecassis K, Rodriguiz RM, Huang XP, Norval S, Sassano MF, Shin AI, Webster LA, Simeons FR, Stojanovski L, Prat A, Seidah NG, Constam DB, Bickerton

GR, Read KD, Wetsel WC, Gilbert IH, Roth BL, Hopkins AL. Automated design of ligands to polypharmacological profiles. Nature 2012;492(7428):215–220. [PubMed: 23235874]

[5]. Blevins JE, Stanley BG, Reidelberger RD. DMSO as a vehicle for central injections: tests with feeding elicited by norepinephrine injected into the paraventricular nucleus. Pharmacol Biochem Behav 2002;71(1–2):277–282. [PubMed: 11812533]

[6]. Boudreau D, Von Korff M, Rutter CM, Saunders K, Ray GT, Sullivan MD, Campbell CI, Merrill JO, Silverberg MJ, Banta-Green C, Weisner C. Trends in long-term opioid therapy for chronic non-cancer pain. Pharmacoepidemiol Drug Saf 2009;18(12):1166–1175. [PubMed: 19718704]

[7]. Brennan TJ, Vandermeulen EP, Gebhart GF. Characterization of a rat model of incisional pain. Pain 1996;64(3):493–502. [PubMed: 8783314]

[8]. Cantuti-Castelvetri L, Ojha R, Pedro LD, Djannatian M, Franz J, Kuivanen S, van der Meer F, Kallio K, Kaya T, Anastasina M, Smura T, Levanov L, Szirovicza L, Tobi A, Kallio-Kokko H, Österlund P, Joensuu M, Meunier FA, Butcher SJ, Winkler MS, Mollenhauer B, Helenius A, Gokce O, Teesalu T, Hepojoki J, Vapalahti O, Stadelmann C, Balistreri G, Simons M. Neuropilin-1 facilitates SARS-CoV-2 cell entry and infectivity. Science 2020;370(6518):856–860. [PubMed: 33082293]

[9]. Carmeliet P, Tessier-Lavigne M. Common mechanisms of nerve and blood vessel wiring. Nature 2005;436(7048):193–200. [PubMed: 16015319]

[10]. Chaplan SR, Bach FW, Pogrel JW, Chung JM, Yaksh TL. Quantitative assessment of tactile allodynia in the rat paw. J Neurosci Methods 1994;53(1):55–63. [PubMed: 7990513]

[11]. Cheng X, Huo J, Wang D, Cai X, Sun X, Lu W, Yang Y, Hu C, Wang X, Cao P. Herbal Medicine AC591 Prevents Oxaliplatin-Induced Peripheral Neuropathy in Animal Model and Cancer Patients. Front Pharmacol 2017;8:344. [PubMed: 28638341]

[12]. Cherny N, Ripamonti C, Pereira J, Davis C, Fallon M, McQuay H, Mercadante S, Pasternak G, Ventafridda V. Strategies to manage the adverse effects of oral morphine: an evidence-based report. J Clin Oncol 2001;19(9):2542–2554. [PubMed: 11331334]

[13]. Chew LA, Bellampalli SS, Dustrude ET, Khanna R. Mining the Nav1.7 interactome: Opportunities for chronic pain therapeutics. Biochem Pharmacol 2019;163:9–20. [PubMed: 30699328]

[14]. Coste B, Crest M, Delmas P. Pharmacological dissection and distribution of NaN/Nav1.9, T-type Ca2+ currents, and mechanically activated cation currents in different populations of DRG neurons. J Gen Physiol 2007;129(1):57–77. [PubMed: 17190903]

[15]. Daly JL, Simonetti B, Klein K, Chen KE, Williamson MK, Antón-Plágaro C, Shoemark DK, Simón-Gracia L, Bauer M, Hollandi R, Greber UF, Horvath P, Sessions RB, Helenius A, Hiscox JA, Teesalu T, Matthews DA, Davidson AD, Collins BM, Cullen PJ, Yamauchi Y. Neuropilin-1 is a host factor for SARS-CoV-2 infection. Science 2020;370(6518):861–865. [PubMed: 33082294]

[16]. De Rossi P, Harde E, Dupuis JP, Martin L, Chounlamountri N, Bardin M, Watrin C, Benetollo C, Pernet-Gallay K, Luhmann HJ, Honnorat J, Malleret G, Groc L, Acker-Palmer A, Salin PA, Meissirel C. A critical role for VEGF and VEGFR2 in NMDA receptor synaptic function and fear-related behavior. Molecular Psychiatry 2016;21(12):1768–1780. [PubMed: 26728568]

[17]. de Vries C, Escobedo JA, Ueno H, Houck K, Ferrara N, Williams LT. The fms-like tyrosine kinase, a receptor for vascular endothelial growth factor. Science 1992;255(5047):989–991. [PubMed: 1312256]

[18]. Di Cesare Mannelli L, Tenci B, Micheli L, Vona A, Corti F, Zanardelli M, Lapucci A, Clemente AM, Failli P, Ghelardini C. Adipose-derived stem cells decrease pain in a rat model of oxaliplatin-induced neuropathy: Role of VEGF-A modulation. Neuropharmacology 2018;131:166–175. [PubMed: 29241656]

[19]. Dib-Hajj SD, Yang Y, Black JA, Waxman SG. The Na(V)1.7 sodium channel: from molecule to man. Nat Rev Neurosci 2013;14(1):49–62. [PubMed: 23232607]

[20]. Diop L, Raymond F, Fargeau H, Petoux F, Chovet M, Doherty AM. Pregabalin (CI-1008) inhibits the trinitrobenzene sulfonic acid-induced chronic colonic allodynia in the rat. J Pharmacol Exp Ther 2002;302(3):1013–1022. [PubMed: 12183658]

[21]. Dubuisson D, Dennis SG. The formalin test: a quantitative study of the analgesic effects of morphine, meperidine, and brain stem stimulation in rats and cats. Pain 1977;4(2):161–174. [PubMed: 564014]

[22]. Dustrude ET, Moutal A, Yang X, Wang Y, Khanna M, Khanna R. Hierarchical CRMP2 posttranslational modifications control NaV1.7 function. Proc Natl Acad Sci U S A 2016;113(52):E8443–e8452. [PubMed: 27940916]

[23]. Dustrude ET, Wilson SM, Ju W, Xiao Y, Khanna R. CRMP2 protein SUMOylation modulates NaV1.7 channel trafficking. J Biol Chem 2013;288(34):24316–24331. [PubMed: 23836888]

[24]. Fan LJ, Kan HM, Chen XT, Sun YY, Chen LP, Shen W. Vascular endothelial growth factor-A/vascular endothelial growth factor2 signaling in spinal neurons contributes to bone cancer pain. Mol Pain 2022;18:17448069221075891.

[25]. Francois-Moutal L, Wang Y, Moutal A, Cottier KE, Melemedjian OK, Yang X, Wang Y, Ju W, Largent-Milnes TM, Khanna M, Vanderah TW, Khanna R. A membrane-delimited N-myristoylated CRMP2 peptide aptamer inhibits CaV2.2 trafficking and reverses inflammatory and postoperative pain behaviors. Pain 2015;156(7):1247–1264. [PubMed: 25782368]

[26]. Friesner RA, Banks JL, Murphy RB, Halgren TA, Klicic JJ, Mainz DT, Repasky MP, Knoll EH, Shelley M, Perry JK, Shaw DE, Francis P, Shenkin PS. Glide: a new approach for rapid, accurate docking and scoring. 1. Method and assessment of docking accuracy. J Med Chem 2004;47(7):1739–1749. [PubMed: 15027865]

[27]. García-Manero M, Alcazar JL, Toledo G. Vascular endothelial growth factor (VEGF) and ovarian endometriosis: correlation between VEGF serum levels, VEGF cellular expression, and pelvic pain. Fertil Steril 2007;88(2):513–515. [PubMed: 17296185]

[28]. Gomez K, Tang C, Tan B, Perez-Miller S, Ran D, Loya S, Calderon-Rivera A, Stratton HJ, Duran P, Masterson KA, Gabrielsen AT, Alsbiei O, Dorame A, Serafini M, Moutal A, Wang J, Khanna R. Stereospecific Effects of Benzimidazolonepiperidine Compounds on T-Type Ca(2+) Channels and Pain. ACS chemical neuroscience 2022;13(13):2035–2047. [PubMed: 35671441]

[29]. Guo HF, Vander Kooi CW. Neuropilin Functions as an Essential Cell Surface Receptor. The Journal of biological chemistry 2015;290(49):29120–29126. [PubMed: 26451046]

[30]. Hamilton JL, Nagao M, Levine BR, Chen D, Olsen BR, Im HJ. Targeting VEGF and Its Receptors for the Treatment of Osteoarthritis and Associated Pain. J Bone Miner Res 2016;31(5):911–924. [PubMed: 27163679]

[31]. Harada T, Takahashi H, Kaya H, Inoki R. A test for analgesics as an indicator of locomotor activity in writhing mice. Arch Int Pharmacodyn Ther 1979;242(2):273–284. [PubMed: 543756]

[32]. Hargreaves K, Dubner R, Brown F, Flores C, Joris J. A new and sensitive method for measuring thermal nociception in cutaneous hyperalgesia. Pain 1988;32(1):77–88. [PubMed: 3340425]

[33]. Hong S, Morrow TJ, Paulson PE, Isom LL, Wiley JW. Early painful diabetic neuropathy is associated with differential changes in tetrodotoxin-sensitive and -resistant sodium channels in dorsal root ganglion neurons in the rat. J Biol Chem 2004;279(28):29341–29350. [PubMed: 15123645]

[34]. Ibrahim MM, Patwardhan A, Gilbraith KB, Moutal A, Yang X, Chew LA, Largent-Milnes T, Malan TP, Vanderah TW, Porreca F, Khanna R. Long-lasting antinociceptive effects of green light in acute and chronic pain in rats. Pain 2017;158(2):347–360. [PubMed: 28092651]

[35]. Jarvis A, Allerston CK, Jia H, Herzog B, Garza-Garcia A, Winfield N, Ellard K, Aqil R, Lynch R, Chapman C, Hartzoulakis B, Nally J, Stewart M, Cheng L, Menon M, Tickner M, Djordjevic S, Driscoll PC, Zachary I, Selwood DL. Small molecule inhibitors of the neuropilin-1 vascular endothelial growth factor A (VEGF-A) interaction. Journal of medicinal chemistry 2010;53(5):2215–2226. [PubMed: 20151671]

[36]. Jensen TS, Baron R, Haanpaa M, Kalso E, Loeser JD, Rice ASC, Treede RD. A new definition of neuropathic pain. Pain 2011;152(10):2204–2205. [PubMed: 21764514]

[37]. Julio-Pieper M, Lozada P, Tapia V, Vega M, Miranda C, Vantman D, Ojeda SR, Romero C. Nerve growth factor induces vascular endothelial growth factor expression in granulosa cells via a trkA receptor/mitogen-activated protein kinase-extracellularly regulated kinase 2-dependent pathway. J Clin Endocrinol Metab 2009;94(8):3065–3071. [PubMed: 19454577]

[38]. Khanna R, Yu J, Yang X, Moutal A, Chefdeville A, Gokhale V, Shuja Z, Chew LA, Bellampalli SS, Luo S, Francois-Moutal L, Serafini MJ, Ha T, Perez-Miller S, Park KD, Patwardhan AM, Streicher JM, Colecraft HM, Khanna M. Targeting the CaValpha-CaVbeta interaction yields an antagonist of the N-type CaV2.2 channel with broad antinociceptive efficacy. Pain 2019;160(7):1644–1661. [PubMed: 30933958]

[39]. Khanna R, Zougman A, Stanley EF. A proteomic screen for presynaptic terminal N-type calcium channel (CaV2.2) binding partners. Journal of biochemistry and molecular biology 2007;40(3):302–314. [PubMed: 17562281]

[40]. Kim BW, Choi M, Kim YS, Park H, Lee HR, Yun CO, Kim EJ, Choi JS, Kim S, Rhim H, Kaang BK, Son H. Vascular endothelial growth factor (VEGF) signaling regulates hippocampal neurons by elevation of intracellular calcium and activation of calcium/calmodulin protein kinase II and mammalian target of rapamycin. Cell Signal 2008;20(4):714–725. [PubMed: 18221855]

[41]. Kroeze WK, Sassano MF, Huang XP, Lansu K, McCorvy JD, Giguère PM, Sciaky N, Roth BL. PRESTO-Tango as an open-source resource for interrogation of the druggable human GPCRome. Nat Struct Mol Biol 2015;22(5):362–369. [PubMed: 25895059]

[42]. Le Bars D, Gozariu M, Cadden SW. Animal models of nociception. Pharmacol Rev 2001;53(4):597–652. [PubMed: 11734620]

[43]. Li Y, North RY, Rhines LD, Tatsui CE, Rao G, Edwards DD, Cassidy RM, Harrison DS, Johansson CA, Zhang H, Dougherty PM. DRG Voltage-Gated Sodium Channel 1.7 Is Upregulated in Paclitaxel-Induced Neuropathy in Rats and in Humans with Neuropathic Pain. J Neurosci 2018;38(5):1124–1136. [PubMed: 29255002]

[44]. Licht T, Goshen I, Avital A, Kreisel T, Zubedat S, Eavri R, Segal M, Yirmiya R, Keshet E. Reversible modulations of neuronal plasticity by VEGF. Proc Natl Acad Sci U S A 2011;108(12):5081–5086. [PubMed: 21385942]

[45]. McCloskey DP, Croll SD, Scharfman HE. Depression of synaptic transmission by vascular endothelial growth factor in adult rat hippocampus and evidence for increased efficacy after chronic seizures. J Neurosci 2005;25(39):8889–8897. [PubMed: 16192378]

[46]. Meissirel C, Almodovar CRd, Knevels E, Coulon C, Chounlamountri N, Segura I, Rossi Pd, Vinckier S, Anthonis K, Deléglise B, Mol Md, Ali C, Dassonville K, Loyens E, Honnorat J, Michotte Y, Rogemond V, Smolders I, Voets T, Vivien D, Berghe PV, Bosch LVD, Robberecht W, Chédotal A, Oliviero S, Dewerchin M, Schmucker D, Thomasset N, Salin P, Carmeliet P VEGF modulates NMDA receptors activity in cerebellar granule cells through Src-family kinases before synapse formation. Proceedings of the National Academy of Sciences 2011;108(33):13782–13787.

[47]. Micheli L, Parisio C, Lucarini E, Vona A, Toti A, Pacini A, Mello T, Boccella S, Ricciardi F, Maione S, Graziani G, Lacal PM, Failli P, Ghelardini C, Di Cesare Mannelli L. VEGF-A/VEGFR-1 signalling and chemotherapy-induced neuropathic pain: therapeutic potential of a novel anti-VEGFR-1 monoclonal antibody. Journal of Experimental & Clinical Cancer Research 2021;40(1):320. [PubMed: 34649573]

[48]. Middeke M, Hoffmann S, Hassan I, Wunderlich A, Hofbauer LC, Zielke A. In vitro and in vivo angiogenesis in PC12 pheochromocytoma cells is mediated by vascular endothelial growth factor. Exp Clin Endocrinol Diabetes 2002;110(8):386–392. [PubMed: 12518248]

[49]. Moutal A, Cai S, Yu J, Stratton HJ, Chefdeville A, Gomez K, Ran D, Madura CL, Boinon L, Soto M, Zhou Y, Shan Z, Chew LA, Rodgers KE, Khanna R. Studies on CRMP2 SUMOylation-deficient transgenic mice identify sex-specific Nav1.7 regulation in the pathogenesis of chronic neuropathic pain. Pain 2020;161(11):2629–2651. [PubMed: 32569093]

[50]. Moutal A, Luo S, Largent-Milnes TM, Vanderah TW, Khanna R. Cdk5-mediated CRMP2 phosphorylation is necessary and sufficient for peripheral neuropathic pain. Neurobiol Pain 2019;5.

[51]. Moutal A, Martin LF, Boinon L, Gomez K, Ran D, Zhou Y, Stratton HJ, Cai S, Luo S, Gonzalez KB, Perez-Miller S, Patwardhan A, Ibrahim MM, Khanna R. SARS-CoV-2 spike protein co-opts VEGF-A/neuropilin-1 receptor signaling to induce analgesia. Pain 2021;162(1):243–252. [PubMed: 33009246]

[52]. Nesic O, Sundberg LM, Herrera JJ, Mokkapati VU, Lee J, Narayana PA. Vascular endothelial growth factor and spinal cord injury pain. J Neurotrauma 2010;27(10):1793–1803. [PubMed: 20698758]

[53]. Neugebauer V, Han JS, Adwanikar H, Fu Y, Ji G. Techniques for assessing knee joint pain in arthritis. Mol Pain 2007;3:8. [PubMed: 17391515]

[54]. Peach CJ, Mignone VW, Arruda MA, Alcobia DC, Hill SJ, Kilpatrick LE, Woolard J. Molecular Pharmacology of VEGF-A Isoforms: Binding and Signalling at VEGFR2. Int J Mol Sci 2018;19(4).

[55]. Perez-Miller S, Patek M, Moutal A, Duran P, Cabel CR, Thorne CA, Campos SK, Khanna R. Novel Compounds Targeting Neuropilin Receptor 1 with Potential To Interfere with SARS-CoV-2 Virus Entry. ACS Chem Neurosci 2021;12(8):1299–1312. [PubMed: 33787218]

[56]. Powell J, Mota F, Steadman D, Soudy C, Miyauchi JT, Crosby S, Jarvis A, Reisinger T, Winfield N, Evans G, Finniear A, Yelland T, Chou YT, Chan AWE, O'Leary A, Cheng L, Liu D, Fotinou C, Milagre C, Martin JF, Jia H, Frankel P, Djordjevic S, Tsirka SE, Zachary IC, Selwood DL. Small Molecule Neuropilin-1 Antagonists Combine Antiangiogenic and Antitumor Activity with Immune Modulation through Reduction of Transforming Growth Factor Beta (TGFβ) Production in Regulatory T-Cells. J Med Chem 2018;61(9):4135–4154. [PubMed: 29648813]

[57]. Ramer MS, Thompson SWN, McMahon SB. Causes and consequences of sympathetic basket formation in dorsal root ganglia. Pain 1999;Suppl 6:S111–s120.

[58]. Ran D, Gomez K, Moutal A, Patek M, Perez-Miller S, Khanna R. Comparison of quinazoline and benzoylpyrazoline chemotypes targeting the CaVα-β interaction as antagonists of the N-type CaV2.2 channel. Channels (Austin) 2021;15(1):128–135. [PubMed: 33416017]

[59]. Randall LO, Selitto JJ. A method for measurement of analgesic activity on inflamed tissue. Arch Int Pharmacodyn Ther 1957;111(4):409–419. [PubMed: 13471093]

[60]. Roux S, Sablé E, Porsolt RD. Primary observation (Irwin) test in rodents for assessing acute toxicity of a test agent and its effects on behavior and physiological function. Curr Protoc Pharmacol 2005;Chapter 10:Unit 10.10.

[61]. Sastry GM, Adzhigirey M, Day T, Annabhimoju R, Sherman W. Protein and ligand preparation: parameters, protocols, and influence on virtual screening enrichments. J Comput Aided Mol Des 2013;27(3):221–234. [PubMed: 23579614]

[62]. Schmalhofer WA, Calhoun J, Burrows R, Bailey T, Kohler MG, Weinglass AB, Kaczorowski GJ, Garcia ML, Koltzenburg M, Priest BT. ProTx-II, a selective inhibitor of NaV1.7 sodium channels, blocks action potential propagation in nociceptors. Mol Pharmacol 2008;74(5):1476–1484. [PubMed: 18728100]

[63]. Skobe M, Hawighorst T, Jackson DG, Prevo R, Janes L, Velasco P, Riccardi L, Alitalo K, Claffey K, Detmar M. Induction of tumor lymphangiogenesis by VEGF-C promotes breast cancer metastasis. Nature Medicine 2001;7(2):192–198.

[64]. Takano S, Uchida K, Inoue G, Matsumoto T, Aikawa J, Iwase D, Mukai M, Miyagi M, Takaso M. Vascular endothelial growth factor expression and their action in the synovial membranes of patients with painful knee osteoarthritis. BMC Musculoskelet Disord 2018;19(1):204. [PubMed: 29945585]

[65]. Taylor RS. Epidemiology of Refractory Neuropathic Pain. Pain Practice 2006;6(1):22–26. [PubMed: 17309705]

[66]. Wang J, He C, Zhou T, Huang Z, Zhou L, Liu X. NGF increases VEGF expression and promotes cell proliferation via ERK1/2 and AKT signaling in Muller cells. Mol Vis 2016;22:254–263. [PubMed: 27081296]

[67]. Willett CG, Boucher Y, di Tomaso E, Duda DG, Munn LL, Tong RT, Chung DC, Sahani DV, Kalva SP, Kozin SV, Mino M, Cohen KS, Scadden DT, Hartford AC, Fischman AJ, Clark JW, Ryan DP, Zhu AX, Blaszkowsky LS, Chen HX, Shellito PC, Lauwers GY, Jain RK. Direct evidence that the VEGF-specific antibody bevacizumab has antivascular effects in human rectal cancer. Nature Medicine 2004;10(2):145–147.

[68]. Xiao Y, Blumenthal K, Jackson JO 2nd, Liang S, Cummins TR. The tarantula toxins ProTx-II and huwentoxin-IV differentially interact with human Nav1.7 voltage sensors to inhibit channel activation and inactivation. Mol Pharmacol 2010;78(6):1124–1134. [PubMed: 20855463]

[69]. Yaksh TL, Rudy TA. Chronic catheterization of the spinal subarachnoid space. Physiol Behav 1976;17(6):1031–1036. [PubMed: 14677603]

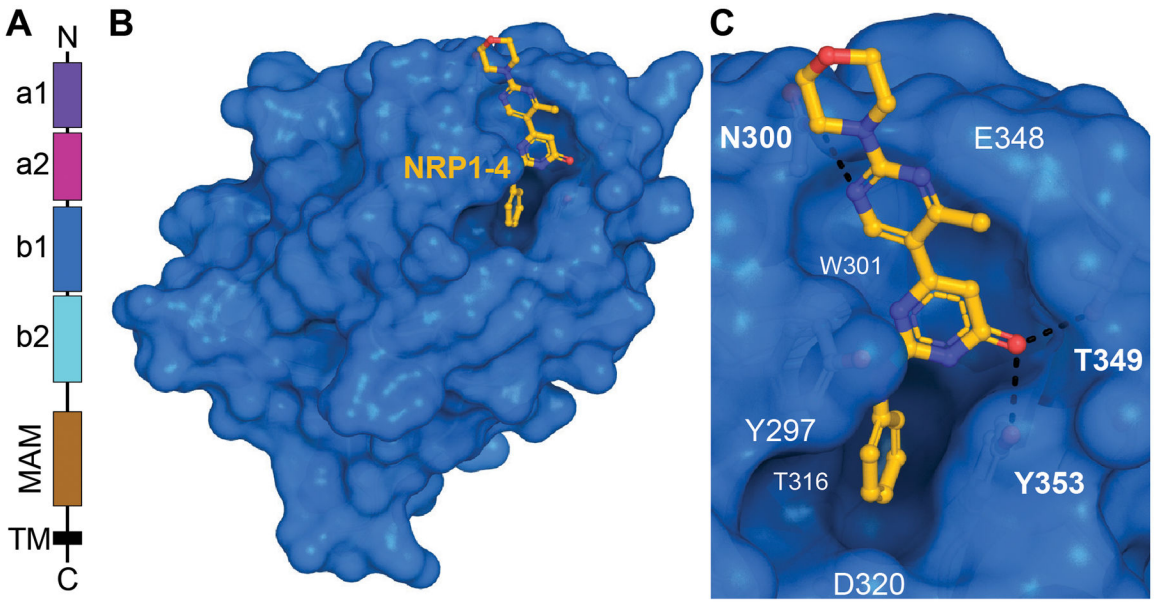

Figure 1 –. Domain structure of NRP1 and docking of NRP1–4 to NRP1.

(A) Domain architecture of NRP1 consists of the extracellular N-terminus (N), tandem CUB domains (a1, a2), tandem F5/8 type C domains (b1, b2), a MAM domain, the transmembrane helix (TM) and the cytoplasmic PDZ domain (C). **(B)** Surface representation of the b1 domain with docked NRP1–4 (gold sticks). **(C)** Close-up of NRP1–4 docked to the VEGF-A CENDR binding pocket. Potential hydrogen bonds indicated with dashed lines. Docking was done as described by Perez-Miller, S., et al. 2021 [55].

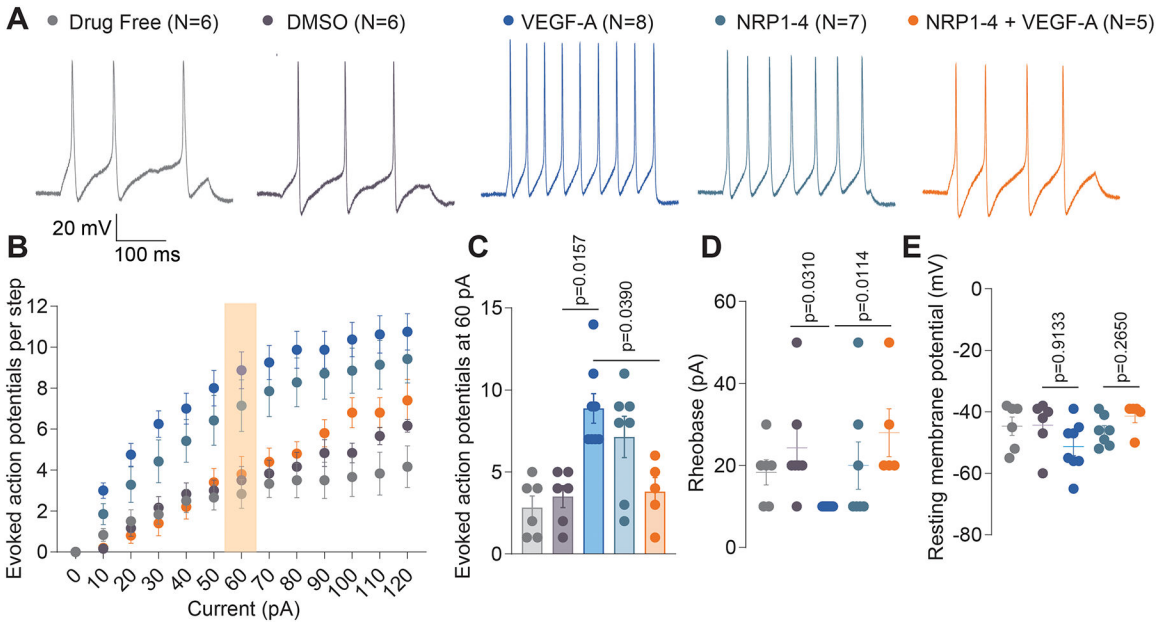

Figure 2 –. VEGF-A increases excitability decreases rheobase of DRG neurons that is blocked by co-treatment with NRP1–4.

(A) Representative traces showing action potentials elicited from DRG neurons following injection of 60pA of depolarizing current into small DRG neurons. Neurons were given either no treatment or treated with the indicated compound/protein. **(B)** Quantification of action potentials evoked by sequentially increasing current steps injected into the soma. Yellow box highlights 60 pA current step where traces were extracted. **(C)** Bar graph comparing of the number of action potentials fired by DRG neurons treated with the indicated compound or protein at 60 pA as highlighted by the yellow box in B. **(D)** Scatter plot showing rheobase, or the current required to fire a single action potential. VEGF-A treatment reduced the rheobase and this was blocked by NRP1–4. **(E)** Scatter plots of the resting membrane potential compared among the groups treated with indicated compounds or proteins. There was no significant difference between the groups for any treatment condition. No-Drug control has nothing added to the recording media. Vehicle was 0.1% DMSO dissolved in the culture media and external recording solution. VEGF-A applied at 1nM and NRP1–4 at 12.5 μM. Data points are mean ± SEM; N as indicated in panel A; Two-way ANOVA used to evaluate statistical differences in (B); Kruskal-Wallis test with Dunn’s multiple comparisons test for panels C-E.

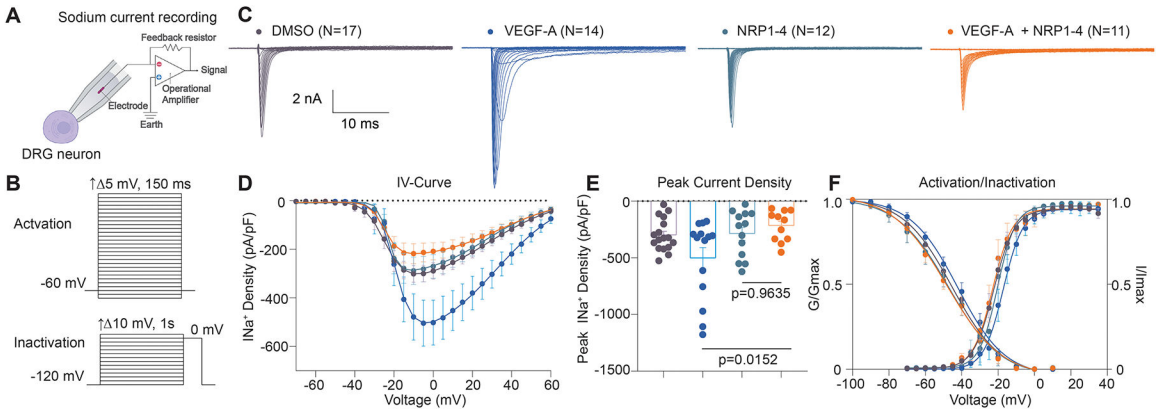

Figure 3 –. Administration of NRP1–4 blocks VEGF-A mediated increase in sodium currents.

(A) Schematic diagram showing the recording configuration for whole-cell patch clamp measurements of isolated DRG neurons. **(B)** Representative current traces obtained from DRG neurons following treatment with the indicated compound or protein. **(C)** Current-density voltage plot for each of the above conditions demonstrating that VEGF-A enhances sodium currents, and that this enhancement can be blocked by co-application of NRP1–4. Current density was obtained by normalizing the inward current measured at each voltage step to cellular capacitance. **(D)** Peak sodium current densities for the indicated treatment conditions indicating that treatment with NRP1–4 blocks the VEGF-A induced increase in current density. **(E)** Voltage dependent activation curves for the above treatment conditions showing that there is no significant change in this measure due to treatment with VEGF-A or NRP1–4. Vehicle was 0.1% DMSO dissolved in the culture media and external recording solution. VEGF-A applied at 1nM and NRP1–4 at 12.5 μM. Data points are mean ± SEM; N as indicated in panel A; statistical differences determined using one-way analysis of variance, which was performed because all data passed the D'Agostino-Pearson test for normality. Biophysical properties reported in Table S2.

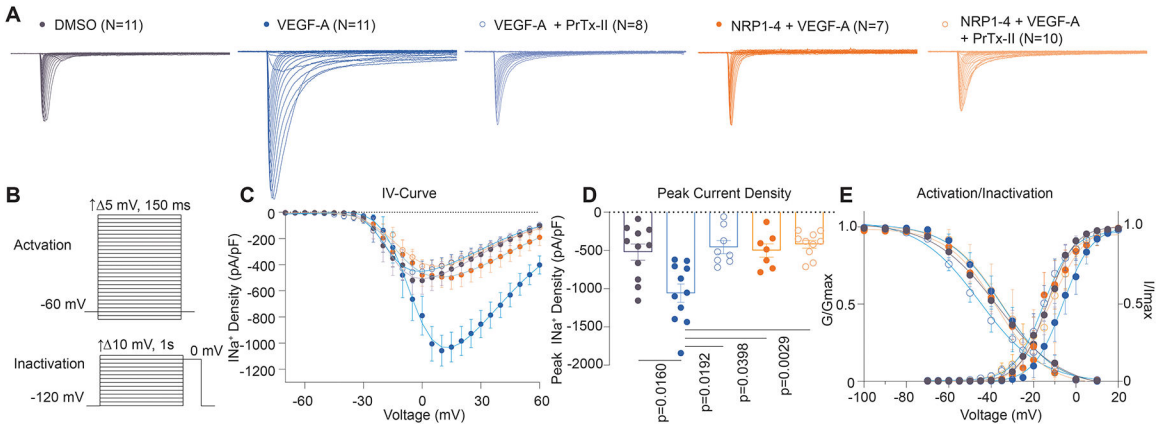

Figure 4 –. VEGF-A mediated increase in DRG sodium currents is due to NaV1.7.

(A) Representative current traces obtained from DRG neurons following treatment with the indicated compound or protein. **(B)** Current-density voltage plot for each of the above conditions demonstrating that VEGF-A enhances sodium currents, and that this enhancement can be blocked by co-application of NRP1–4. This VEGF-A dependent increase in sodium current is reduced by co-treatment with PrTx-II (5 nM), a selective NaV1.7 inhibiting peptide. Current density was obtained by normalizing the inward current measured at each voltage step to cellular capacitance. **(D)** Peak sodium current densities for the indicated treatment conditions illustrating that treatment with NRP1–4 blocks the VEGF-A induced increase in current density. No further decrease is seen when NRP1–4 is applied in combination with VEGF-A and PrTx-II. **(E)** Voltage dependent activation curves for the above treatment conditions showing that there is no significant change in this measure due to treatments applied. Vehicle was 0.1% DMSO dissolved in the culture media and external recording solution. VEGF-A applied at 1nM, NRP1–4 at 12.5 μM, and PrTx-II at 5nM (in PBS). Data points are mean ± SEM; N as indicated in panel A; statistical differences determined Kruskal-Wallis test followed by Dunn's multiple comparisons test, All distributions were assessed with the D'Agostino-Pearson test for normality. Biophysical properties reported in Table S2.

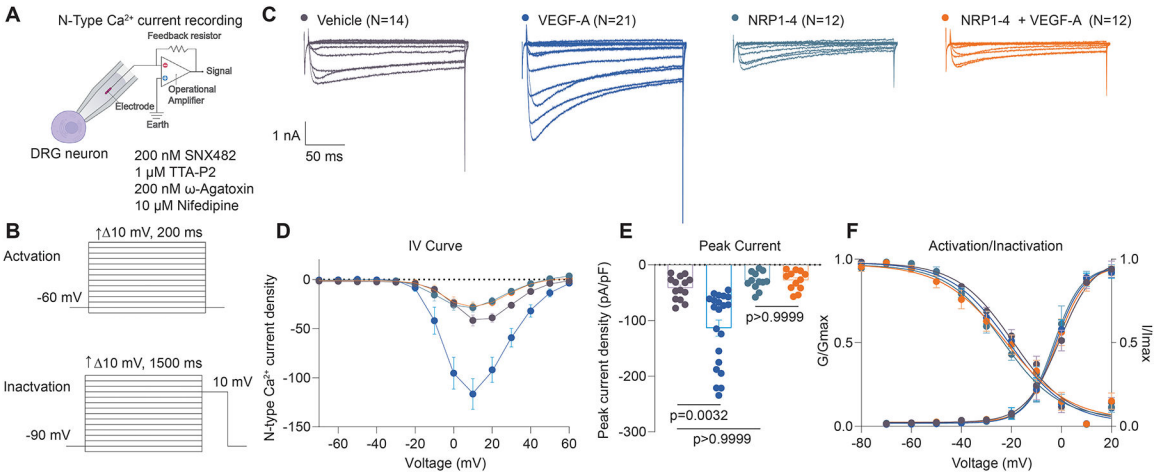

Figure 5 –. NRP1–4 blocks VEGF-A mediated increase in N-type calcium currents.

(A) Schematic diagram showing the recording configuration for whole-cell patch clamp measurements of isolated sensory neurons in the presence of calcium channel blockers to isolate N-type calcium currents. **(B)** Diagram depicting the voltage protocols used to elicit currents from DRG neurons and investigate the properties of activation and inactivation of voltage-gated calcium channels. **(C)** Representative current traces obtained from DRG neurons following treatment with the indicated compound or protein. **(D)** Current-density voltage plot for each of the above conditions demonstrating that VEGF-A enhances N-type calcium currents, and that this enhancement can be blocked by co-application of NRP1–4. Current density was obtained by normalizing the inward current measured at each voltage step to cellular capacitance. **(E)** Peak calcium current densities for the indicated treatment conditions illustrating that treatment with NRP1–4 blocks the VEGF-A induced increase in N-type current density. Treatment with NRP1–4 alone had no effect on N-type peak current density. **(F)** Voltage dependent activation curves and steady state fast inactivation for the above treatment conditions showing that there is no significant change in these biophysical channel properties due to treatment with VEGF-A or NRP1–4. Vehicle was 0.1% DMSO dissolved in the culture media and external recording solution. VEGF-A applied at 1nM and NRP1–4 at 12.5 μM. Toxins used were dissolved in DMSO or PBS and the same amount of each solvent was added to the vehicle condition. Data points are mean ± SEM; N as indicated in panel C; statistical differences determined using Mann-Whitney test after performing D'Agostino-Pearson test for normality. Biophysical properties reported in Table S2.

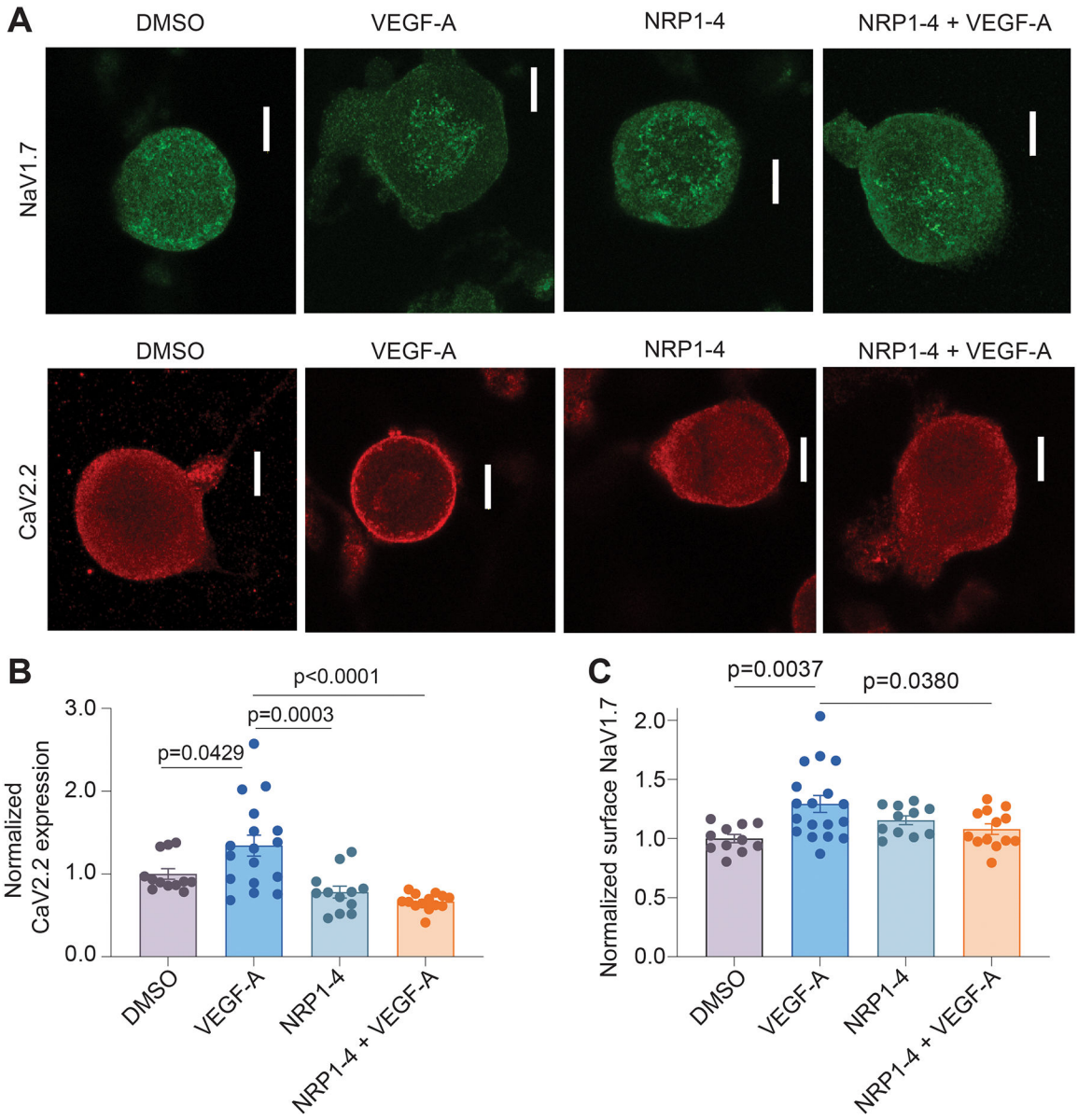

Figure 6 - NRP1–4 prevents VEGF-A mediated increase in CaV2.2 and NaV1.7 surface expression in rat DRG neurons.

(A) Representative confocal images of rat DRG neuron cultures following treatment with the indicated protein or compound and labeled with an antibody against CaV2.2 or NaV1.7. Scale bar: 10 μm. (B) Quantification of normalized surface expression of CaV2.2 per neuron shows that treatment with NRP1–4 compound blocks the VEGF-A induced increase in surface expression of CaV2.2. Treatment with NRP1–4 alone had no effect. (C) Quantification of normalized surface expression of NaV1.7 for individual neurons illustrating that treatment with NRP1–4 also blocks the VEGF-A induced increase in surface expression of NaV1.7. Vehicle was 0.1% DMSO dissolved in the culture media and external recording solution. VEGF-A applied at 1nM and NRP1–4 at 12.5 μM. Data points are mean ± SEM; One-way ANOVA test with Holm-Sidak multiple comparisons for (B) and Tukey's multiple comparison post hoc test for (C); N= 11–18 cells per group

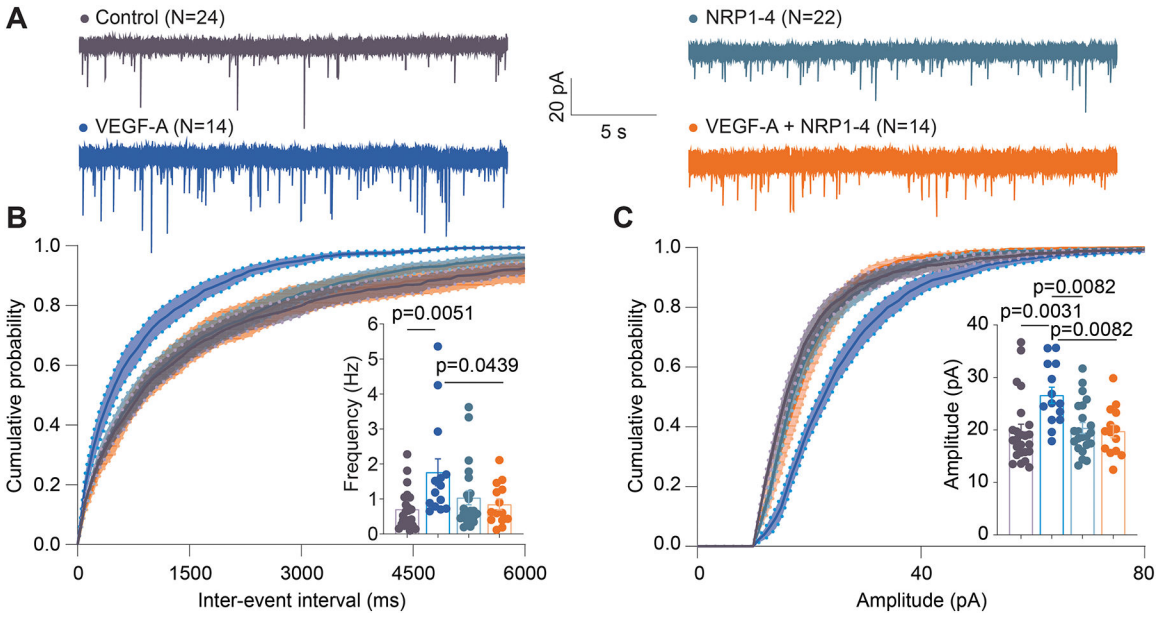

Figure 7 –. NRP1–4 reverses VEGFA-mediated increase in frequency of spontaneous excitatory postsynaptic currents in the lumbar dorsal horn.

(A) Representative traces of sEPSC recordings from substantia gelatinosa (SG) in the superficial dorsal horn (lamina I/II) treated for at least 30 minutes with the indicated conditions: VEGFA (4 nM), NRP1–4 (VEGFA/NRP1 binding inhibitor, 12.5 μM), or both. **(B)** Cumulative distribution of sEPSC inter-event intervals recorded from SG neurons. Inset: Bar graph with scatter plot showing sEPSC frequency. **(C)** Cumulative distribution of sEPSC amplitudes intervals recorded from SG neurons. Inset: Bar graph with scatter plot showing sEPSC amplitude. Addition of VEGFA increased sEPSC frequency in the SDH but selective knockdown of VEGFA/NRP1 interaction with NRP1–4 compound blocked this effect. Vehicle was 0.1% DMSO and PBS dissolved in the external recording solution. VEGF-A applied at 4 nM and NRP1–4 at 12.5 μM. Data are expressed as mean ± SEM. One way ANOVA with Tukey's post hoc test for multiple comparisons. For full statistical analyses, see Table S1.

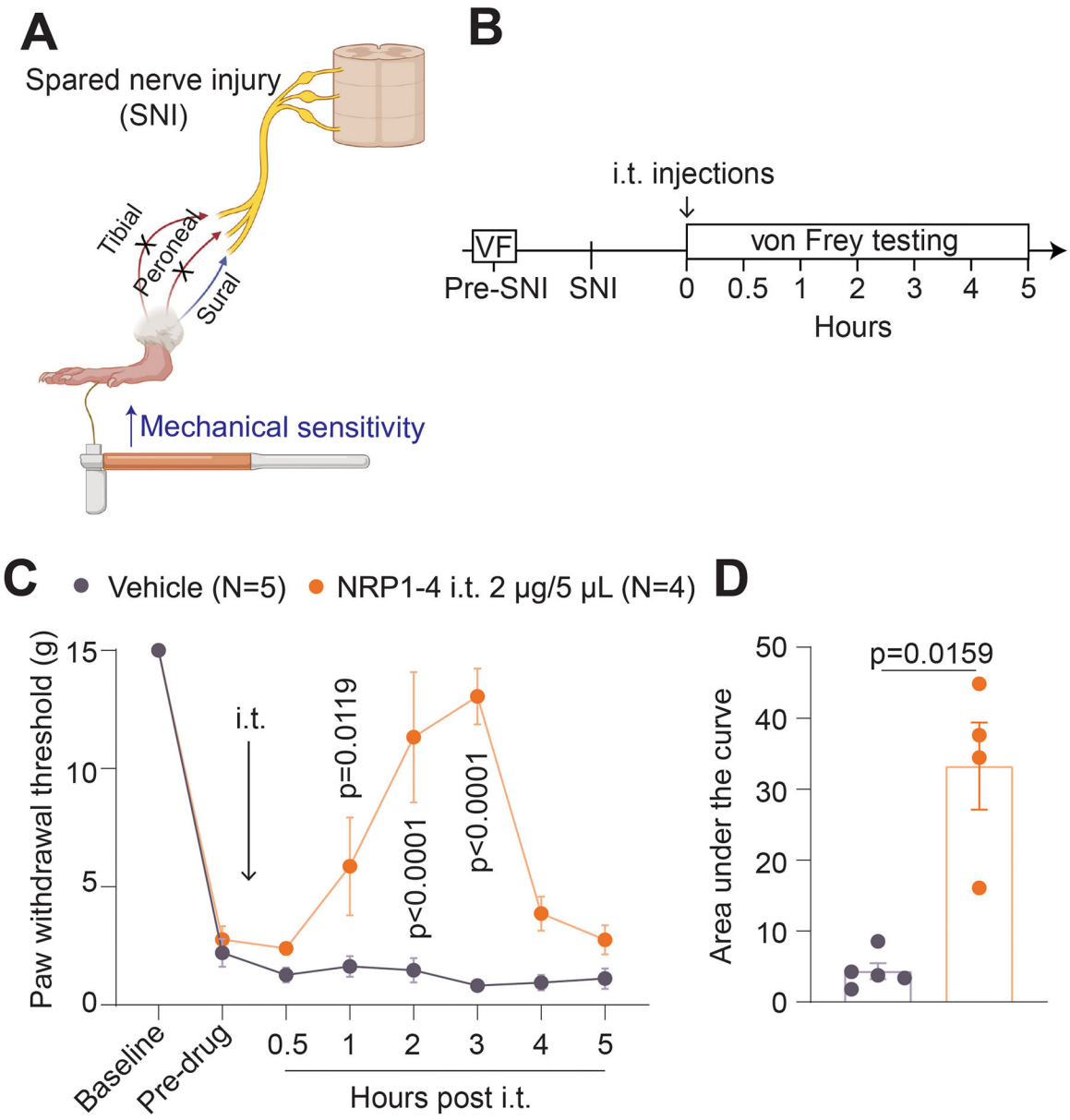

Figure 8 –. Intrathecal injection of NRP1–4 reverses mechanical allodynia following spared nerve injury.

(A) Diagram representing the spared nerve injury (SNI) paradigm where the common peroneal and tibial nerves are ligated but the sural nerve is left intact. This model of neuropathic pain produces robust and highly reproducible hypersensitivity on the side ipsilateral to the injury. **(B)** Timeline of the experimental paradigm indicating that pre-SNI baseline measurements of withdrawal threshold were taken before nerve injury. Animals were then randomly assigned to a treatment group and on the day of the injection mechanical allodynia was verified. An intrathecal injection was then administered using an implanted catheter extending to the lumbar level of the spinal cord and withdrawal thresholds were followed for five hours post injection. **(C)** Central administration of NRP1–4 reverses mechanical hypersensitivity associated with nerve injury for three hours following

treatment. **(D)** Quantification of the area bounded by the curve and the x-axis to compare the total reversal of hypersensitivity between groups. This comparison shows a robust reversal of mechanical allodynia following treatment with NRP1–4. Vehicle was 0.1% DMSO dissolved in sterile saline for injection, which is the same ratio of DMSO used to dissolve NRP1–4 for the drug treated group. Data points are mean ± SEM; N as indicated in panel C; Statistical differences determined using nonparametric two-way ANOVA with time as the within subject factor and treatment as the between subject factor and Sidak's posthoc test for multiple comparisons; Differences in area under the curve were determined using the Mann-Whitney test. The experiments were conducted by an experimenter blinded to the treatment condition For full statistical analyses, see Table S1.

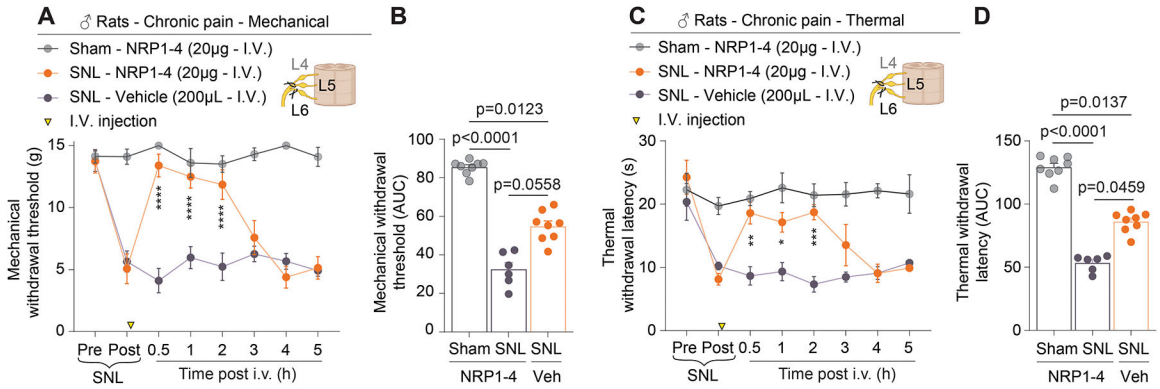

Figure 9 –. NRP1–4 is antinociceptive following spinal nerve ligation.

Ligature of L5 and L6 spinal nerves (SNL) was performed in male rats to induce chronic neuropathic pain. Sham surgeries were performed without any ligation. Two weeks post-surgery, animals were administered saline solution (vehicle) or NRP1–4 (20 µg) through intravenous (i.v.) injections (200 µL). Yellow triangles indicate the time of i.v. injections. **(A)** Mechanical sensitivity was evaluated over 5 hours using von Frey filament test. **(B)** Area under the curve analysis for mechanical withdrawal thresholds presented in panel A. NRP1–4 provided antinociception in rats subjected to chronic neuropathic pain (n=6–8, Kruskal Wallis test followed by Dunn's multiple comparisons posthoc test). **(C)** Thermal sensitivity was evaluated over 5 hours using Hargreaves test. **(D)** Area under the curve analysis for thermal withdrawal latencies presented in panel C. NRP1–4 provided antinociception in rats subjected to chronic neuropathic pain (n=6–8, Kruskal Wallis test followed by Dunn's multiple comparisons posthoc test). Values represent mean ± standard error of the mean. *p<0.05, **p<0.01, ***p<0.001, ****p<0.0001 for SNL-NRP1–4 vs SNL-Saline. The experiments were conducted by an experimenter blinded to the treatment conditions. For full statistical analyses, see Table S1.